11-2-2020

Formation and Repair of Environmentally-induced damage to Mitochondrial and Nuclear Genomes

Yunhee Ji
yji008@fiu.edu

FLORIDA INTERNATIONAL UNIVERSITY

Miami, Florida

FORMATION AND REPAIR OF ENVIRONMENTALLY-INDUCED DAMAGE TO MITOCHONDRIAL AND NUCLEAR GENOMES

A dissertation submitted in partial fulfillment of

the requirements for the degree of

DOCTOR OF PHILOSOPHY

in

PUBLIC HEALTH

by

Yunhee Ji

2020

To: Dean Tomás R. Guilarte
R.Stempel College of Public Health and Social Work

This dissertation, written by Yunhee Ji, and entitled Formation and Repair of Environmentally-induced Damage to Mitochondrial and Nuclear Genomes, having been approved in respect to style and intellectual content, is referred to you for judgment.

We have read this dissertation and recommend that it be approved.

Stanislaw F. Wnuk

Lidia Kos

Quentin Felty

Kim Tieu

Helen Tempest

Marcus S. Cooke, Major Professor

Date of Defense: November 2, 2020

The dissertation of Yunhee Ji is approved.

Dean Tomás R. Guilarte
R.Stempel College of Public Health and Social Work

Andrés G. Gil
Vice President for Research and Economic Development
and Dean of the University Graduate School

Florida International University, 2020

DEDICATION

I dedicate my dissertation to my lovely family. My parents Mr. Young-Ki Ji and Mrs. Gwangil Byun always support me with unconditional love and inspiration. My sister EunHee Ji and Kyunghwan Ji support me all the way through my dissertation with care and love.

ACKNOWLEDGMENTS

Firstly, I would like to express my sincere gratitude to my major advisor Dr. Marcus Cooke, for providing me an opportunity to work in OSG group, all his support and great supervision during my Ph. D study and research. He is a great advisor and mentor. Without his support and supervision, this dissertation would not have been possible.

Besides my major advisor, I would like to thank my thesis committee: Dr. Stainslaw Wnuk, Dr. Quentin Felty, Dr. Kim Tieu, Dr. Lidia Kos, and Dr. Helen Tempest for their comments, concern, and encouragement during five years of my Ph.D. study. I am really thankful for the valuable advice during the committee meetings, which helped me to develop critical thinking about the research. I would like to acknowledge and thank Dr. Mahsa Karbaschi for teaching and advising everything in the lab for four years. I also thank to collaborators from Newcastle University, Dr. Mark Birch-Machin and Dr. Rebecca Hanna to provide us good PCR method protocols, and Dr. Alhegaili Alaa for performing and publishing paper using DDIP-seq.

I also thank all my lab mates and friends. In particular, I thank Hadi Abdulwahed, the best lab mate, and friend, for the days working, studying, and all the fun we have had during my five years in the lab.

I would like to thank the Department of Environmental Health Sciences and Robert Stempel College of Public Health & Social Work for the graduate assistantship. I also would like to thank the University graduate school for the Dissertation Year Fellowship award.

ABSTRACT OF THE THESIS

FORMATION AND REPAIR OF ENVIRONMENTALLY-INDUCED DAMAGE TO MITOCHONDRIAL AND NUCLEAR GENOMES

by

Yunhee Ji

Florida International University, 2020

Miami, Florida

Professor Marcus S. Cooke, Major Professor

All living organisms are continually exposed to various environmental stressors, be they anthropogenic or natural in origin. Many stressors share a common toxic mechanism, generating highly reactive chemical species that can have detrimental effects. A proportion of these chemical species evade the cell's defenses and damage cellular components, including DNA. Measurement of global genome levels of DNA and cellular damage has implicated environmental stressors in major human health issues (e.g., cancer, aging, cardiovascular, and neurodegenerative diseases). Current associations between DNA damage and disease are based upon crude assessments of global genome damage, which provide limited mechanistic information on how damage leads to disease. Furthermore, DNA damage is not uniformly distributed across the genome; accumulation, or persistence, of damage in regions of the genome vital to the functioning of the cell, will have downstream consequences. Thus, we proposed, that the role of DNA damage in disease can only be understood by examination of damage in the context of its location and damage response during the repair. Currently we lack information concerning how the cell maintains baseline levels of DNA damage and its spatio-temporal distribution across the

genome. This is fundamental to our understanding of how the cell responds to damage and whether regions are targeted for prioritized repair. In this study, we have refined a popular method of assessing global DNA damage, to increase the efficiency of the assay, mapped UV-induced T<>T across both nuclear and mitochondrial genomes, and evaluated the changes in the cellular DNA damage response during bacterial infection. The aim of these studies was to evaluate the importance of cellular response to exposure to environmental toxicants.

TABLE OF CONTENTS

CHAPTER PAGE

LIST OF TABLES

TABLE PAGE

LIST OF FIGURES

FIGURE PAGE

ABBREVIATIONS AND ACRONYMS

8-oxoGua	8-oxo-7,8-dihydroguanine
Ade	Adenine
ACA	Alkaline comet assay
ALS	Alkali labile sites
BE-M17	Dopaminergic neuroblastoma cells
BER	Base excision repair
bp	Base pair
BSA	Bovine serum albumin
Cyt	Cytosine
Ct	Threshold cycle
CPD	Cyclobutane pyrimidine dimers
DDIP-seq	Damaged DNA immunoprecipitation sequencing
DMEM	Dulbecco's modified eagle medium
DMSO	Dimethylsulphoxide
DNA	Deoxyribonucleic acid
dsDNA	Double-stranded DNA
EDTA	Ethylenediaminetetraacetic acid
ELISA	Enzyme-linked immunosorbent assay
FBS	Fetal bovine serum
GG-NER	Global genome nucleotide excision repair
Gua	Guanine
h	hour
HaCaTs	Immortalized human keratinocytes
HCl	Hydrochloric acid
hOGG1	Human 8-oxoguanine DNA glycosylase

HPLC-MS/MS	High performance liquid chromatography with tandem mass- spectrometric
LMP	Low melting point
IQR	Interquartile range
mg	Milligram
min	Minute
MMR	Mismatch repair
mtDNA	Mitochondrial DNA
MTH1	Mut T homologue 1
NaCl	Sodium chloride
nDNA	Nuclear DNA
NER	Nucleotide excision repair
ng	Nanogram
OGG1	8-oxoguanine DNA glycosylase
O/N	Overnight
PBS	Phosphate buffer saline
PCR	Polymerase chain reaction
pH	Potential of Hydrogen
PI	Propidium iodide
qPCR	Quantitative polymerase chain reaction
ROS	Reactive oxygen species
RT	Room temperature
SB	DNA strand breaks
SD	Standard deviation
SEM	Standard error of the mean
SSR	Solar simulated radiation
Thy	Thymine
T4endoV	T4 endonuclease V

TC-NER	Transcription-coupled nucleotide excision repair
T<>T	Cyclobutane thymine dimer
U	Unit
UV	Ultraviolet
UVA	Ultraviolet A
UVB	Ultraviolet B
UVC	Ultraviolet C
UVR	Ultraviolet radiation
V	Voltage
µL	Micoliter
µM	Micromolar
%TD	Percentage tail DNA (DNA damage)

REFACE

The following chapters have been published and have been formatted for those publications.

CHAPTER 3

Karbaschi, M., Ji, Y., Abdulwahed, A. M. S., Alohaly, A., Bedoya, J. F., Burke, S. L., ... & Cooke, M. S. (2019). Evaluation of the Major Steps in the Conventional Protocol for the Alkaline Comet Assay. *International Journal of Molecular Sciences*, ***20***(23), 6072.

CHAPTER 4

Alhegaili, A. S., Ji, Y., Sylvius, N., Blades, M. J., Karbaschi, M., Tempest, H. G, ... & Cooke, M. S. (2019). Genome-Wide Adductomics Analysis Reveals Heterogeneity in the Induction and Loss of Cyclobutane Thymine Dimers across Both the Nuclear and Mitochondrial Genomes. *International journal of molecular sciences*, ***20***(20), 5112.

CHAPTER 5

Ji, Y., Karbaschi, M., & Cooke, M. S. (2019). Mycoplasma infection of cultured cells induces oxidative stress and attenuates cellular base excision repair activity. *Mutation Research/Genetic Toxicology and Environmental Mutagenesis,* 845, 403054.

CHAPTER 1

Environmentally induced DNA damage, repair, and disease

1.Nuclear and mitochondrial DNA in mammalian cells

Eukaryotic organisms contain two kinds of deoxyribonucleic acid (DNA) in two different sites, the nucleus, and mitochondria. Nuclear DNA (nDNA) and mitochondrial DNA (mtDNA) are both in the form of a double helix, with two DNA strands composed of sugar (2-deoxyribose), a phosphate group, and four nucleobases [Thymine (Thy), Adenine (Ade), Cytosine (Cyt) and Guanine(Gua)] (Figure 1.1) [1]. The bases are composed of carbon and nitrogen ring, and they are separated into two groups- purines (double-rings; Ade and Gua) and pyrimidines (single ring; Cyt and Thy), as shown in Figure 1.2 [2]. As a Chargaff rule and Watson -Crick base-pairing rules in double-stranded DNA (dsDNA), purines naturally pair with pyrimidines by hydrogen bonds and form nucleotides with a phosphate group via a phosphodiester bond. For example, guanine bonds with cytosine by forming three hydrogen bonds, and adenine binds to thymine by forming two hydrogen bonds [3].

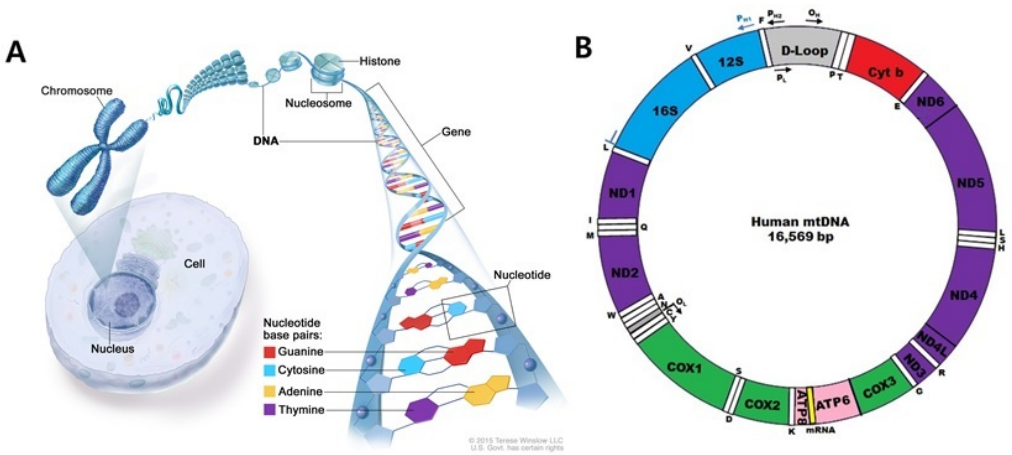

(National Cancer Institute/Terese Winslow, 2015)

Figure 1. 1 Illustration of the structure of (A) nuclear DNA and (B) mitochondrial DNA

Three nucleotides encode one amino acid, and in the human genome, nDNA is linear in shape and has 3.3 billion base pairs with 46 chromosomes that encode 20,000 to 25,000 genes [4].

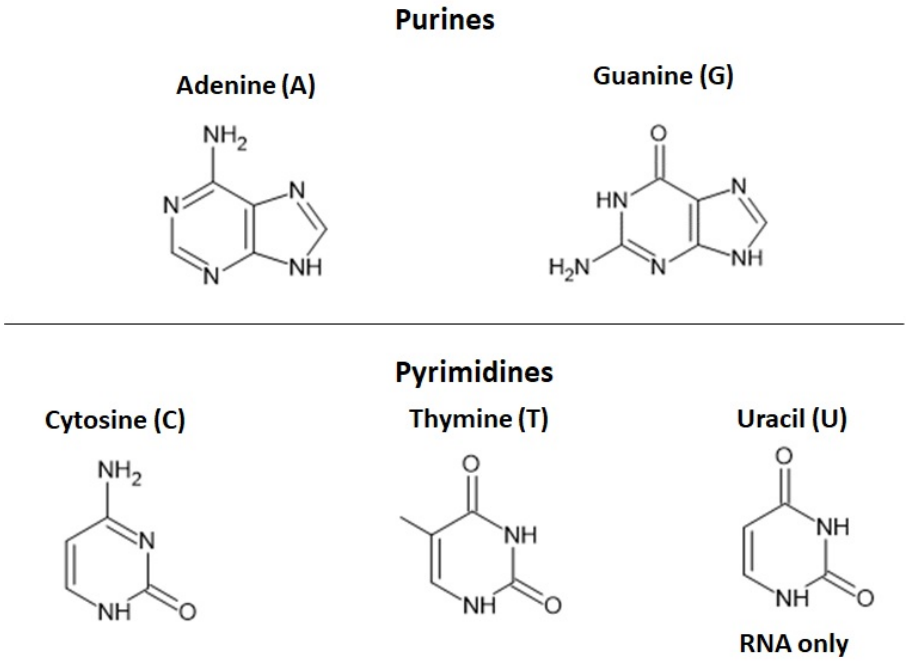

Figure 1. 2 Structure of nucleobases

Compared to the nDNA, mtDNA is circular in shape, and it is in the mitochondrial matrix within the mitochondrial inner membrane. mtDNA comprises 16,569 base pairs with 37 genes of which 13 genes encode protein subunits associated with respiratory complexes that are important for the respiratory chain in mitochondria [5, 6]. Both nDNA and mtDNA encode genes that play an important role in cell function and metabolism. Therefore, damage, and mutations, to either nDNA or mtDNA, may be associated with pathogenesis in humans. In this chapter, environmental factors that cause DNA damage, the cellular response to the damage, and lead the diseases related to nDNA and mtDNA damage will be introduced.

2. Environmentally induced DNA damage

Many types of DNA damage and the resulting mutations occur due to exogenous and endogenous factors. Strand breaks, modified nucleobases, bulky DNA adducts, and abasic sites are common types of DNA damage found in nDNA and mtDNA [7]. Endogenous factors such as reactive oxygen species (ROS) are produced by metabolism and could induce DNA damage in the cells – particularly under oxidative stress, where the balance between prooxidants and antioxidants is tipped in favor of the former. Exogenous factors can also be a source of oxidative stress in the cell. There are many kinds of exogenous factors inducing a variety of DNA damage in cells.

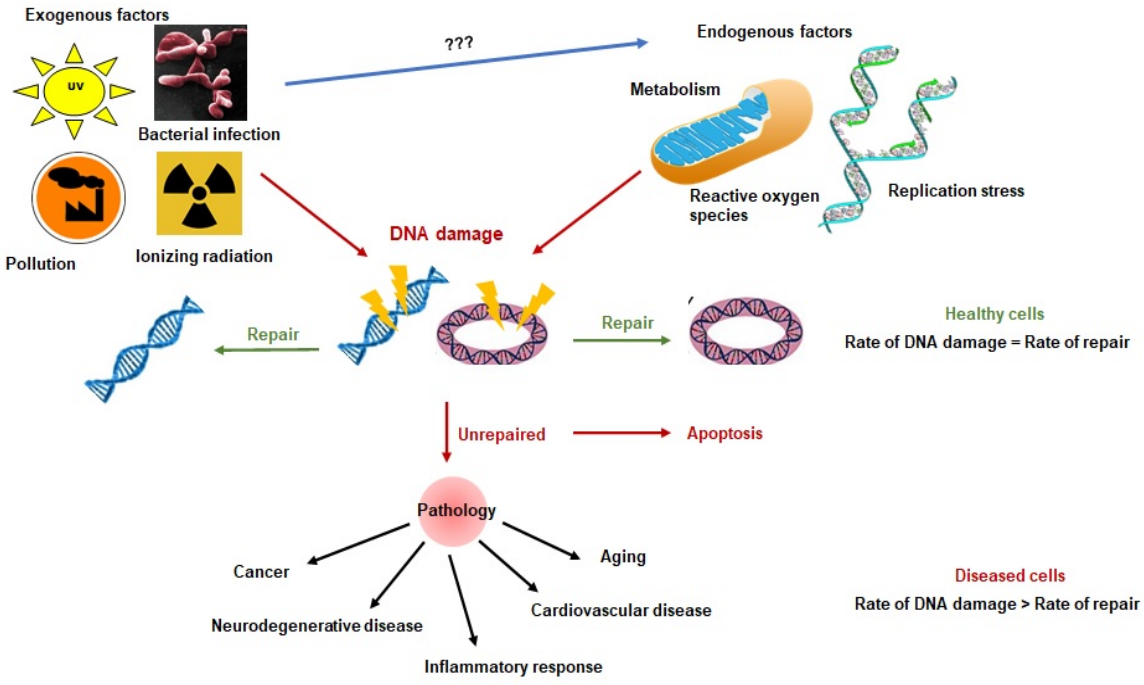

Figure 1. 3 Overview of DNA damage, repair, and pathogenesis. Exogenous factors and endogenous factors induce DNA damage. Once DNA is damaged, damaged DNA is repaired using a cellular repair mechanism. However, increases in the rate of DNA damage leads to diseases such as cancer, aging, and neurodegenerative diseases.

Ultraviolet radiation (UVR) is one of the well-known exogenous factors that produce bulky adducts (e.g. cyclobutane thymine dimers: T<>T) in both nDNA and mtDNA and can also induce ROS that leads to oxidation of nDNA and mtDNA. In this section, exogenous factors that cause DNA damage will be introduced.

2.1 Oxidative stress- induced DNA damage (an example of non-bulky adducts)

Oxidative stress is one of the factors that cause DNA damage. ROS are chemically reactive molecules containing oxygen, and they are produced by natural metabolism, essential for biological function, cell signaling, cell survival, growth, proliferation, and differentiation [8]. ROS, such as superoxide or the hydroxyl radical, react with DNA and cause DNA damage by breaking the DNA double strands, together with other forms of damage, such as modification of the nucleobases [9]. This damage can lead to DNA mutation and potentially induce carcinogenesis, or apoptosis, or lead to cellular aging [10, 11]. In addition to DNA, ROS can cause oxidation in the 2'-deoxyribonucleotide pool. For example, UVA irradiation is a factor that produces ROS by interaction with intracellular photosensitizer that induces ROS in the cells [12]. Once dGTP is oxidized by ROS, it forms 8-oxodGTP, which may be misincorporated into into G:C > C:G and G:C > T:A transversions during DNA replication [13]. The oxidized purine, 8-oxo-7,8-dihydro-2'-deoxyguanosine (8-oxodG) is described as a non-bulky adduct (as it is only a subtle modification of dG, compared to other adducts, such as pyrimidine dimers), and it is a widely recognized biomarker of oxidative stress. It is also a major DNA damage product of ROS and oxidative stress [13].

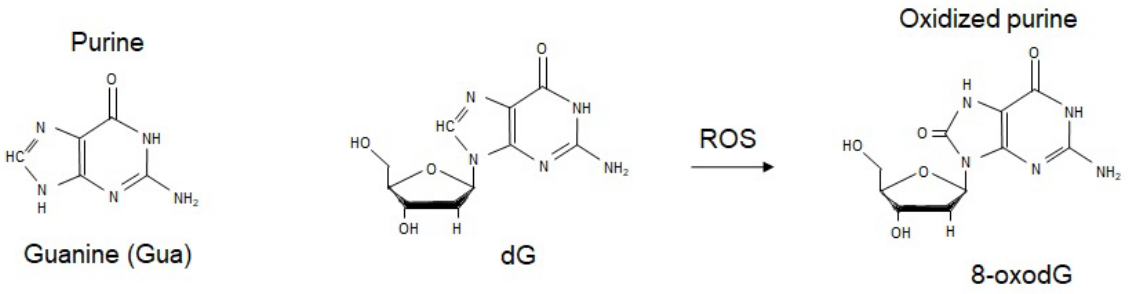

Figure 1. 4 Example of the formation of oxidized purines

2.2 UV induced DNA damage – Pyrimidine dimers (an example of a bulky adducts)

UVR, some chemicals, and ionizing radiation are examples of the exogenous factors that induce DNA damage. UVR is classified into three categories based upon wavelength: UVA (320-400 nm), UVB (280-320 nm), and UVC (200-280 nm) [14]. Although UVR has some beneficial properties, in terms of producing vitamin D in humans, UVR is a most effective inducer of DNA damage and mutations, which can lead to skin carcinogenesis, by forming cyclobutane pyrimidine dimers (CPD), arising from the formation of bonds between C5 and C6 in pyrimidine bases [14-17]. The distribution and formation of DNA damage induced by UVR depend on multiple factors, such as DNA sequences, structure, and chromatin organization, in part due to the sequence specificity of UVR and access of DNA repair enzyme to the adducts [18-20]. Failure to repair CPD causes DNA mutation and skin cancer.

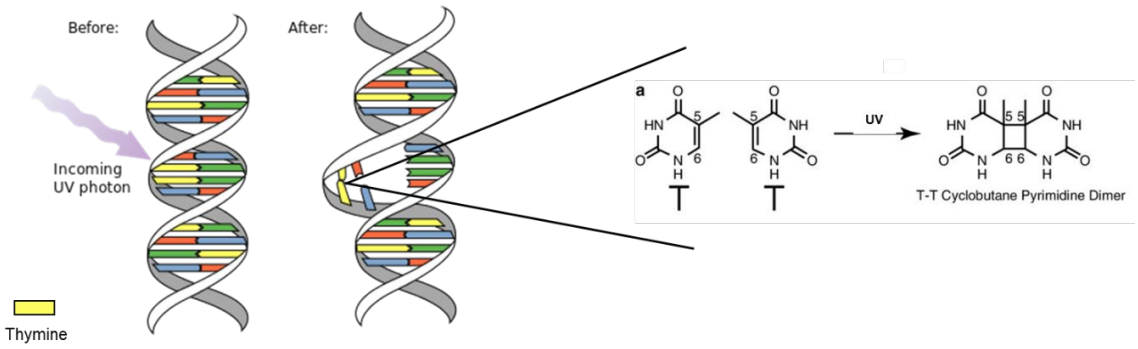

(NASA/Herring, Wikipedia, 2010)

Figure 1. 5 Formation of CPD after UV radiation exposure of DNA

2.3 Bacterial infection- Mycoplasma as a potential environmental source of DNA damage

Mycoplasma is a bacterium that lacks a cell wall surrounding the cell membrane, and because of this biological feature, it makes them markedly different from other bacteria [21]. The absence of a cell wall, coupled with their small size, allows Mycoplasma to pass through sterilizing filters that would otherwise prevent contamination [21]. It also makes Mycoplasma resistant to antibiotics, which require binding to the cell wall of a bacterium for their effect. Common sources of contamination that lead to Mycoplasma infection include cell culture supplies, reagents, exposure to other Mycoplasma contaminated cells, or laboratory supplements [21, 22]. Mycoplasma causes altered metabolism, morphological changes, and changes in cell growth and viability (which can increase or decrease) [23]. However, the precise effects of Mycoplasma contamination on specific host cell functions remain unclear, partly because the Mycoplasma genus contains many different species, each of which has a different effect on host cell function [23]. It has been reported that Mycoplasma infections in humans lead to oxidative stress, by causing the

changes in protein levels that are associated with a respiratory response, and the induction dsDNA breaks [24]. Furthermore, Mycoplasma changes the expression of a plethora of genes, modifying the cellular responses of the host cells, and rendering the results of such an *in vitro* cell model invalid.

3. DNA repair

Protecting the cells and rescuing DNA from damage is the repair of damaged DNA using a variety of DNA repair pathways. There are many repair pathways to correct DNA damage such as nucleotide excision repair (NER) and base excision repair (BER).

3.1 Nuclear excision repair (NER)

NER removes damaged nucleobases within a string of nucleotides and is particularly targeted towards bulky lesions. As such, this pathway is the most critical pathway to remove CPD [25, 26]. NER has two different sub-pathways to recognize DNA damage: global genome NER (GG-NER) and transcription-coupled NER (TC-NER). GG-NER operates across the entire genome, however TC-NER focuses on actively transcribed regions in the genome. The reason behind this is a mechanism for the recognition of DNA damage (Figure 3.1). GG-NER recognizes bulky adducts using xeroderma pigmentosum C protein (XP-C) and 23 B protein complex. This complex recruits TFIIH, a transcription factor that contains a helicase subunit that helps unwind damaged DNA. XP-G and RPA protein bind to the DNA repair complex to destabilize the helix until the complex bubble holds about 25 nucleobases. After the complex covers 25 nucleobases, endonuclease XP-F and XP-G cut the damaged strand fragment, and DNA polymerase fills the gap, and DNA ligase seals the nick [27]. In contrast, TC-NER uses RNA polymerase to recognize the

damaged DNA by getting blocked by DNA adduct. Once blocked by the adduct, a small protein called CSB binds to the damaged site and recruits XP-G to unwind the helix, and the same pathway as GG-NER proceeds to remove and repair the damaged DNA [27].

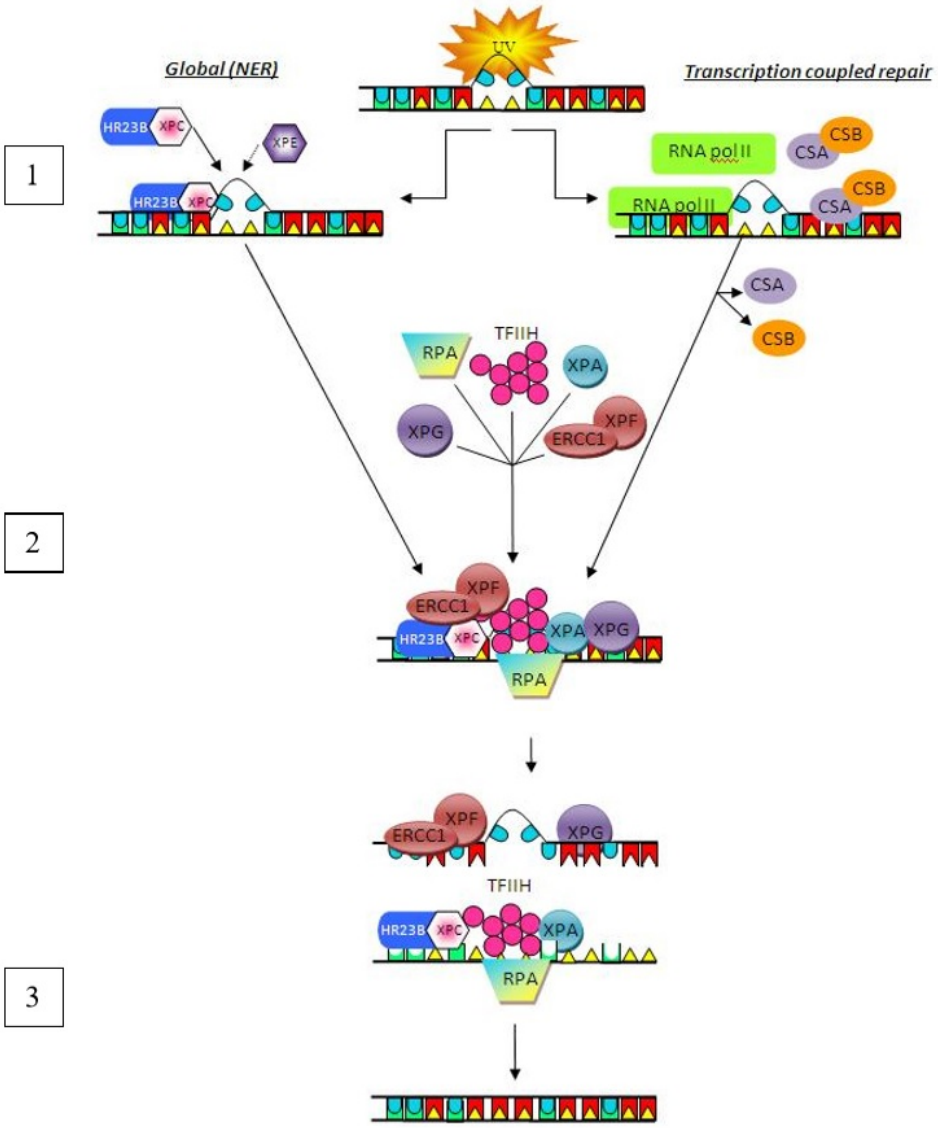

(Karbaschi, 2012)

Figure 1. 6 The pathways of Global genome and Transcription-coupled nuclear excision repair

3.2 Base excision repair (BER)

Base excision repair (BER) repairs damaged DNA by removing the damaged nucleobase [28]. Thus, BER is also important in preventing mutations, and there are a number of pathways to achieve this, each involving different BER enzymes, with overlapping substrates. Human 8-oxoguanine DNA glycosylase (hOGG1) is the primary enzyme for removing oxidized purines. For example, it removes 8-oxo-7,8-dihydroguanine (8-oxoGua) when formed *in situ*, opposite cytosine [29]. In contrast, human mutY homologue (hMYH) removes adenine when it is mispaired with 8-oxoGua. Excising adenine from opposite the damaged DNA nucleobase provides an additional opportunity for the correct nucleobase to be inserted (i.e. cytosine), and then create the substrate for the 8-oxoGua to be repaired by hOGG1 [30, 31]. There are two BER pathways, long-patch BER and short-patch BER. DNA glycosylases such as hOGG1 cleaves 8-oxoGua when paired with cytosine and form an AP site (apurinic/aprimidinic site). AP endonuclease cleaves AP sites when they are formed. After AP site formation, Short- patch BER removes the damaged nucleotide while long-patch BER eliminates the damaged nucleotide, together with a number of undamaged nucleotides (Figure 3.2) [32]. Mitochondrial DNA is easily damaged by ROS due to the proximity to ROS generation within the mitochondria. Failure to convert superoxide to hydrogen peroxide causes oxidation of mtDNA resulting in oxidized purines, such as 8-oxoGua [33]. Once mtDNA is damaged, the mtDNA repair systems are activated. There are many mtDNA repair pathways, although BER and Mismatch repair (MMR) is the most common repair systems. BER is one of the most important routes to repair oxidatively damaged mtDNA.

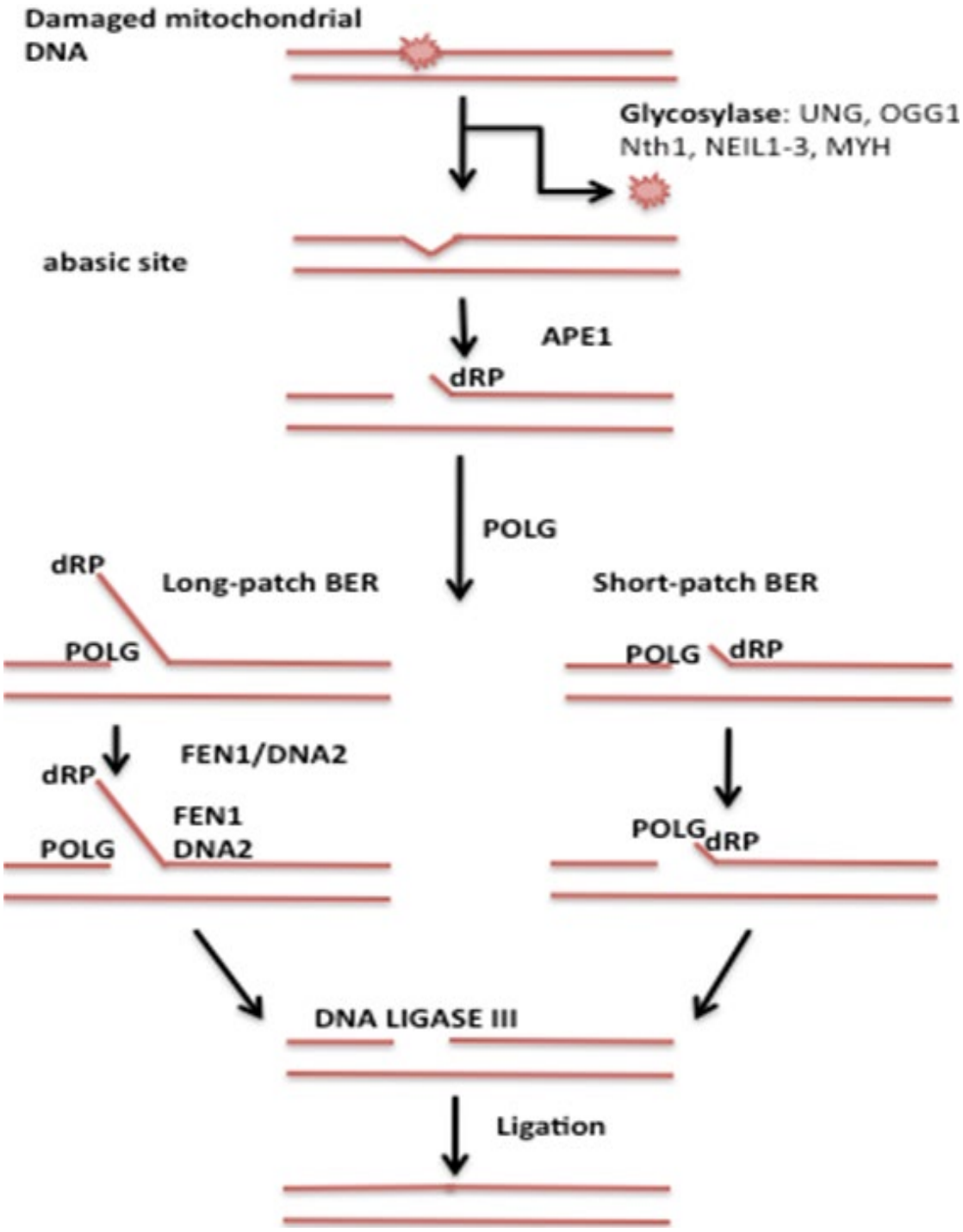

(Martin, 2011)

Figure 1. 7 Summary of mitochondrial DNA BER process

3.3 Mismatch repair (MMR)

Mismatch repair (MMR) is one of the pathways that corrects the misincorporation of nucleobases (base-pair mismatch, nucleotide insertion, and deletion) during DNA replication [34]. For example, in human cells, there are two heterodimers involved in MMR: bacterial *MutS* homolog alpha (MSH2/MSH6α: MutSα) and beta (MSH2/MSH3β: MutSβ) [35]. MutSα is involved in the small insertion and deletion of mispaired nucleotides (one or two nucleotides), but MutSβ is involved the longer insertion (one to 15 mispaired nucleotides) [35]. If there is a mismatched nucleotide synthesized in the daughter strand during DNA replication, MutS protein recognizes mismatched nucleotides, and it binds to the mispaired segment. After MutS proteins bind and form the DNA-protein complex, it recruits MutL homolog alpha (MLH1/PMS2α: MutLα) required for MMR. MutLα, a repair endonuclease, binds to the DNA-MutS protein complex, and it distinguishes template strand and newly synthesized daughter strand that contained mispaired nucleotides [36]. MutL nick the mispaired daughter strand and recruits DNA helicase (MCM9) and replication protein RPA to unwind the mismatched nucleotide and excise the mismatched segment by Exonuclease 1 (EXO1) [37]. After excision, DNA polymerase δ re-synthesizes the nucleotides, and DNA ligase fills the gaps [38].

4. Diseases in which DNA damage is implicated

4.1 Neurodegenerative diseases

Environmental toxicants and stress increase the risk of neurodegeneration disease. Glyphosate, which is a toxic herbicide, decreases zinc levels in the brain, which causes neurological toxicity [39]. Much of the toxin mechanisms implicated in neurodegeneration appear to be linked to the induction of oxidative stress and its consequences. For examples,

exposure to glyphosate increases H_2O_2 levels in cells, which causes oxidative stress, and is closely associated with cytotoxicity and neurodegenerative disease [40]. This coupled with the high levels of iron in the substantia nigra, or low levels of glutathione, increase the likelihood of oxidative stress, which will then form $^{\bullet}OH$ from the H_2O_2, a mechanism implicated Parkinson's disease. Free radicals induce aggregation of soluble beta-amyloid (Aβ) into insoluble plaques, which are associated with Alzheimer's disease [41]. Deficiency in the DNA repair enzyme Ape1 (human AP endonuclease) has been reported to lead to apoptosis in oxidatively damaged neuronal cells [42]. Furthermore, lower levels of hOGG1 activity are found in the brain tissue of Alzheimer's disease patients compared with controls [43]. Mice OGG1 and MTH1 work together to suppress 8-oxoGua formation to protect the brain from neurodegeneration. Mice OGG1 deficiency leads to increases in 8-oxoGua levels, which may lead to neurodegenerative disease [44].

4.2 Cancer

Many studies show that environmental exposures are a major cause of cancers. UVR is an example of a well-known environmental factor that causes skin cancer. UVB-exposed human keratinocytes demonstrate increased CC to TT mutations in the *p53* gene (tumor suppressor gene) with increasing the UV dose [45]. Failure to repair T<>T increases the risk of skin cancer. For example, xeroderma pigmentosum (XP) patients have mutation that result in defective NER, as a result these individuals are extremely photosensitive have a higher risk of having skin cancer [46]. In an epidemiological study, the skin cancer incidence rate in general population is significantly correlated with UV exposure [47]. In addition, nearly 65 % of melanoma skin cancers are linked to sun exposure [48].

Another environmental factor linked to cancer is bacterial infection and there is evidence that this occurs via perturbation of the DNA damage response. For example, Mycoplasma chaperone protein DnaK downregulates the DNA repair protein PARP (poly-ADP ribose polymerase-1), and results in the accumulation of DNA damage, and promotion of cellular transformation, PARP also reduces the effect of anticancer drugs such as Nutlin-3 [49]. Benign human prostate BPH-1 cells infected with Mycoplasma develop anchorage-independent growth [50]. Furthermore, nude mice inoculated with Mycoplasma infected BPH-1 cells developed tumors [50]. Many studies have shown the importance of DNA repair pathways in cancer causation and prevention. For example, levels of hMTH1, which is one of the proteins in the NUDT family and hydrolyzes 8-oxodGTP to 8-oxodGMP to prevent misincorporation into DNA, are elevated in lung cancer cells so it helps cells to survive exposure to oxidative stress [51]. Likewise, many studies show the relationship between DNA repair and cancer, or neurodegenerative diseases. However, the consequences of specific types or genomic location of DNA damage or types of DNA repair dysfunction, are not well understood.

5. Techniques that detect DNA damage

Many methods have been used to evaluate and investigate the DNA damage and repair such as single-cell gel electrophoresis (the comet assay), polymerase chain reaction (PCR), and damaged DNA immunoprecipitation sequencing (DDIP-seq). Theses assays have particular strengths and weaknesses, which lend them to specific applications in the field of genotoxicity (Table 1).

5.1 Single-cell gel electrophoresis (the comet assay)

The comet assay is a sensitive method to evaluate the genotoxicity in individual cells [52]. Östling and Johansson developed the comet assay in 1984 [53]. In 1988, the comet assay was developed as a sensitive method to measure low levels of nuclear DNA damage in individual cells [54]. Nowadays, many epidemiology, genotoxicology studies have used the comet assay as a technique to test genotoxicity and human biomonitoring [55]. There are several variants of the comet assay: (1) alkaline comet assay, (2) neutral comet assay, (3) enzyme-modified comet assay. The alkaline comet assay is performed under alkaline conditions with high pH (pH>13) during electrophoresis to detect strand breaks and alkali-labile sites (such as AP sites). The neutral comet assay uses more neutral conditions (pH 8.3), to detect frank single strand breaks, and double strand breaks [56, 57]. The enzyme modified comet assay is used to gain more specificity for the type of DNA damage detected through the use of a specific enzyme (e.g., hOGG1, which removes oxidized purines, and T4endoV, which nicks at CPD). The activity of these enzymes results in breaks at the site of each DNA lesion, which can be detected in the alkaline comet assay.

However, the process of the conventional comet assay is time-consuming, can only run a relatively limited number of samples, and requires a large space in which perform the assay. For these reasons, many high-throughput methods are developed. The COMPAC-50 (Cleaver Scientific Ltd) and CometChip (Trevigen, Inc) are recent examples of high-throughput comet assay platforms with a reduction in buffer usage, duration of performing the assay with a high number of samples [58, 59]. Even though there are many advantages in both COMPAC-50 and CometChip, some limitations still exist with both methods, and

the comet assay in general, such as not being able to analyze mitochondrial DNA damage, and measuring global nuclear DNA damage, with no information on the sites of damage.

5.2 Polymerase chain reaction (PCR)

PCR methods have been used to identify the DNA damage in individual and multiple genes in both nDNA and mtDNA. The mechanism to evaluate DNA damage is to amplify the specific gene that is damaged or undamaged DNA. The concept of PCR to detect DNA damage in the gene of interest is to quantify the PCR product after assay. If there is damage in the gene of interest, the polymerase may be blocked by the adduct or strand break. Therefore, the quantity of PCR products in damaged DNA, will be less than undamaged DNA. But because the amount of PCR product will depend not only on the quality of the DNA (how much damage is present), but also the amount of template DNA i.e. the number of mitochondria, it is important to correct for mitochondrial copy number. This too can be achieved by PCR. The concept of mtDNA contents analysis is to determine the relative copy number using the single-copy gene of damaged nDNA and mtDNA versus undamaged [60]. There is another method to evaluate the DNA damage in multiple genes (up to 30 kb) called long-range PCR [61]. Long-range PCR has been used to investigate depletion, mutations, and the formation of DNA damage in human mitochondria and nuclear DNA [62]. This method is more sensitive than short range PCR methods as the likelihood of encountering damage is a larger region of DNA is greater. PCR methods are sensitive methods to measure region and gene-specific damage, however some kinds of DNA damage are not detectable because the polymerase bypasses the damage, instead of being blocked by it [63].

5.3 Immunoprecipitation sequencing (IP-seq)

Immunoprecipitation sequencing has been used in recent studies to assess DNA damage. Chromatin immunoprecipitation sequencing (ChIP-seq) and damaged DNA immunoprecipitation sequencing (DDIP-seq) are the most commonly used to evaluate DNA damage. ChIP-seq is used to isolate the regions where a DNA repair enzyme binds (DNA protein interaction region). For example, if DNA is damaged and 8-oxoGua is formed, hOGG1 binds to the DNA to perform repair. The hOGG1 is fixed in place by crosslinking, the DNA fragments, and the hOGG1-containing fragments isolated using an anti-hOGG1 antibody. The isolated regions can then be sequenced. For the DDIP-seq, 8-oxoGua containing fragments are isolated directly using anti-8-oxoGua antibody.

Currently, mapping methods (such as DDIP-seq) of gene-specific damaged DNA regions are available at a high resolution. These methods allow the study of the formation and repair of a variety of different kinds of DNA damage (e.g. CPD, oxidized purines, and strand breaks) [64-67]. DDIP-seq is a very reliable and sensitive method with high resolution (100-1000 bp) to detect specific sites, but it is costly [68].

Table 1. Advantages and limitations of the techniques assessing DNA damage.

Method		Advantage		Limitation
Comet assay		• Sensitive method to detect nuclear DNA damage, repair, and cross-links in vivo and in vitro model. • Good method to test genotoxicity of drugs • Inexpensive • Fast, and simple method		• Only detect nuclear DNA damage • Data analysis is time consuming
PCR	Short range	• 80 – 200 bp (efficient amplicon size) • DNA damage detection of specific genes	• Sensitive method to detect nuclear and mitochondrial DNA damage • Region and gene specific	• Time consuming • Analyze one area each time • Required specific primer • Expensive • Some types of DNA damage is not detectable
	Long range	• Up to 20 kb (efficient amplicon size) • DNA damage detection of longer region		
DDIP-seq		• Highly sensitive method to find the DNA damage and mutation • Detection of specific mutation or DNA damage		• Specific antibody needed • Time consuming • Expensive

6. Central hypothesis and specific aims

Many environmental factors cause DNA damage and cellular dysfunction, if not repaired and are therefore implicated in the etiology of numerous diseases. In this thesis, **we hypothesized that different environmental factors induce various types of DNA damage and this leads to a differential response.** To prove this hypothesis, we tested three different aims to examine the DNA damage response in appropriate cell culture models exposed to relevant environmental stressors.

Aim 1. To develop, optimize, and evaluation methods for assessing DNA damage

Aim 2. To investigate the distribution of damage and repair across the nuclear mitochondrial genomes in human skin keratinocytes exposed to UVR and SSR.

Aim 3. To investigate the effect of chronic bacterial infection on the DNA damage response in a model of dopaminergic neurons.

CHAPTER 2
Materials and Methods

Materials

2.1 Cell culture conditions and treatments

2.1.1 Cell culture conditions

2.1.1.1 Human Keratinocytes (HaCaTs)

Immortalized human keratinocytes (HaCaTs) were used as a relevant, representative cell culture model to study the UV induced nuclear and mitochondrial DNA damage and repair. Cells were cultured as a monolayer in cell culture flasks in Dulbecco's Modified Eagle Medium (DMEM): F-12 (1:1) without L-Glutamine (Quality Biological, Gaithersburg, MD, USA) supplemented with 10 % fetal bovine serum (Gibco, Waltham, MA, USA), 2 mM Glutamax (Gibco, Waltham, MA, USA) and 1 mM sodium pyruvate (Gibco, Waltham, MA, USA) without antibiotics, at 37 °C, in a 5 % CO_2 humidified incubator. Cells were sub-cultured at 70 % confluency. Cells were washed twice with PBS before trypsinization to detach them from the flask. 0.25 % Trypsin EDTA was added to the flask and incubated for 10 min at 37 °C in a 5 % CO_2 humidified incubator. Cells were washed with HaCaT media and centrifuged at 300 x g for 5 min. Cells were sub-cultured with a 1:5 ratio.

2.1.1.2 Dopaminergic neuroblastoma cell line (BE-M17)

Dopaminergic neuroblastoma cells (BE-M17) were used as a representative cell culture model to study the effect of Mycoplasma infection on the nuclear and mitochondrial DNA damage response. BE-M17 cells were cultured as a monolayer in cell culture flasks in Dulbecco’s modified Eagle’s medium (Gibco, Waltham, MA, USA) supplemented with 10% fetal bovine serum (Gibco, Waltham, MA, USA), without antibiotics, at 37 °C, in a 5% CO_2 humidified incubator. Cells were sub-cultured 80 % confluency. Cells were

washed with PBS twice prior to the trypsinization with 0.25 % Trypsin EDTA for 1 min at 37 °C in a 5 % CO_2 humidified incubator. Cells were then de-trypsinized with BE-M17 complete media and centrifuged at 300 x g for 5 min. Cell pellets were collected and subculture with a ratio of 1:4.

Mycoplasma contamination testing was performed regularly using 4 mL of cell culture medium from the cells, and a PCR-based method shown as developed and performed by the Tissue Culture Core Facility at Florida International University.

2.1.2 Cell treatment

2.1.2.1 UV irradiation

To induce pyrimidine dimers in cells, UV irradiation was performed in an AirClean 600 PCR workstation cabinet (Airclean System, Creedmoor, NC, USA). UVP UVX Radiometer with three different sensors (Analytik Jena US LLC, Beverly, MA, USA) for each treatment [UVX 25 (UVC), 31 (UVB) or 36 (UVA)] was used to measure UVA, UVB, or UVC intensity prior to irradiation and calculated required dose for UVA, UVB or UVC according to the formula below:

[Exposure time (sec) = Required dose (J/cm^2)/ UV intensity (W/cm^2)]

After two washes of the cells with PBS, cells were irradiated in PBS, adherent, on ice, without the lid of Petri-dishes. After removing the PBS, the cells were washed twice with PBS prior to being trypsinized with 0.25 % Trypsin EDTA (Gibco, Waltham, MA, USA).

2.1.2.2 H_2O_2 treatment

$H_2O_2$was used s a representative inducer of oxidatively generated DNA damage. Cells seeded in 6 well plates or 100 mm Petri dishes and were washed twice prior to H_2O_2 treatment. 50 μM H_2O_2 diluted in serum-free Dulbecco's Modified Eagle Medium

(DMEM): F-12 (1:1) without L-Glutamine (Quality Biological, Gaithersburg, MD, USA) was used to treat cells, on ice, for 30 min in a cell culture cabinet. The cells were trypsinized with 0.25 % Trypsin EDTA (Gibco, Waltham, MA, USA) following the cell culture conditions mentioned in section 2.1.1.

General methods

2.2 DNA damage detection methods

2.2.1 Detection of nuclear DNA damage - the alkaline comet assay

2.2.1.1. Cell preparation for the comet assay

After irradiation described in section 2.1.2.1, cells were trypsinized following the condition for each cell line described in section 2.1. After the centrifugation, 1 mL of PBS was added to the cells, and cell counting performed using trypan blue and a hemocytometer to harvest approximately 30,000 live cells. 30,000 cells were transferred to a 1.5 mL microcentrifuge tube prior to comet assay.

2.2.1.2 Standard alkaline comet assay protocol

200 µL of 0.6 % low melting agarose was added into the cell pellets containing ~30,000 cells. 80 µL of 0.6 % low melting agarose gel, containing ~12,000 cells, were added to pre-chilled, 1 % normal agarose pre-coated microscope slides, and left to solidify under a coverslip on a chilling plate (Cleaver, Rugby, Warwickshire, UK). The coverslips were then removed, and the slides were placed in COMPAC50 slide racks (Cleaver, Rugby, Warwickshire, UK), transferred to a COMPAC50 lysis buffer box (Cleaver, Rugby, Warwickshire, UK) containing lysis buffer (100 mM Na_2EDTA, 2.5 M NaCl, 10 mM Tris-HCl, pH 10) with 1 % Triton X (Sigma, St. Louis, MO, USA) and incubated at 4 °C

overnight. Slides were transferred to a wash box containing cold ddH2O for 20 min and transferred to a COMPAC50 electrophoresis tank (Cleaver, Rugby, Warwickshire, UK) (Figure 2.1) containing electrophoresis buffer (300 mM NaOH, 1 mM Na_2EDTA, pH ≥ 13). Following incubation for 20 min, electrophoresis was performed (1.19 V/cm) for 20 min. The slide-containing racks were then transferred sequentially to tanks containing neutralization buffer (0.4 Tris-HCl, pH 7.5; 20 min); cold ddH_2O (20 min); propidium iodide (2.5 μg/mL) for 20 min in the dark, i.e., with tank lid closed); and finally washed in cold ddH_2O (20 min). After the final wash, the slides were dried before the analysis of comets using Comet IV software, version 4.2 (Perceptive, Shawnee, KS, USA**).**

(Karbaschi et al. 2016)

Figure 2. 1 The COMPAC50 equipment.

2.2.2 Detection of mitochondrial DNA damage - polymerase chain reaction (PCR)

2.2.2.1 Cell culture preparation for DNA extraction

Cells were grown in T75 flasks or 100 mm Petri dishes prior to DNA extraction. Cells were washed twice with PBS and trypsinized with 0.25 % Trypsin EDTA for 10 min (HaCaTs) or 1 min (BE-M17) at 37 °C in a 5 % CO_2 humidified incubator. After trypsinization, completed media was added to the cells to inactivate trypsin. Cells were transferred to a 50 mL falcon tube and centrifuged at 300 x g for 5 min. After removing the supernatant, 1 mL of PBS was added to the cell pellets, and cell counting was performed. Following the cell counting, each required cell number (~30,000 cells) was transferred to a 1.5 mL microcentrifuge tube, and centrifugation was performed for 5 min at 500 x g. PBS was removed, and the cell pellets were stored at -20 °C until DNA extraction was performed.

2.2.2.2 DNA extraction and pre-quantification

DNA extraction was performed using the QIAamp DNA mini kit (Qiagen, Hilden, Germany), and procedures were followed by the manufacture's protocol. Briefly, approximately 5 x 10^6 cells were collected from cell culture. Cells were transferred to a 1.5 mL microcentrifuge tube and centrifuged for 5 min at 300 x g. After centrifugation, the supernatant was removed and resuspended with 200 µL PBS. 20 µL of protein kinase K and 200 µL of lysis buffer were added and mixed by purse vortex for 15 sec. The tubes containing the mixture were then incubated in a heating block for 10 min at 56 °C. Short centrifugation was performed to remove any drops from the lid. 200 µL of isopropanol was added to the tube and mixed by pulse vortex. The mixture was transferred to the column provided in the kit and centrifuged at 6000 x g for 1 min. 2 mL of collection tube

was replaced to the new one, 500 µL of AW1 buffer (washing buffer) was added to the column, and the centrifugation was performed at 6000 x g for 1 min. A new 2 mL collection tube was replaced, 500 µL of AW2 buffer was added to the column and centrifuged at 20,000 x g for 3 min. A new 2 mL tube was replaced with a new tube and centrifuged with 20,000 x g for 1 min. The column was transferred to a 1.5 mL tube, and 200 µL of AE buffer (elution buffer) was added to the column and incubated for 5 min. Centrifugation was performed at 6000 x g for 1 min, and DNA was collected. After DNA extraction, samples were quantified using a Nanodrop (Nanodrop one,[c] Thermofisher, Waltham, MA, USA).

Table 2 Primer sequences and conditions for mtDNA damage detection methods

Primer	Sequence 5'-3'	Amplicon size (bp)	Annealing temperature (°C)	PCR cycles
Short mito Fragment Forward	5'-CCC CAC AAA CCC CAT TAC TAA ACC CA-3'	221	62	25
Short mito Fragment Reverse	5' -TTT CAT CAT GCG GAG ATG TTG GAT GG-3'			

2.2.2.3 Short-range polymerase chain reaction

LongAmp™ Taq 2X Master Mix (NewEngland Biolabs, Ipswich, USA) was used to evaluate cellular mtDNA damage and repair. The primers and conditions used are described in Table 1. The Master mix was prepared per well (with 15 ng DNA) containing 0.4 µM Forward primer, 0.4 µM Reverse primer, 1X LongAmp Taq 2X

Master mix, and made up to 24 µL with nuclease-free water. After samples and master mix were added to the 96 well plate, 25 cycles of the PCR were run using a Mastercycler ® Pro PCR machine (Eppendorf, Germany).

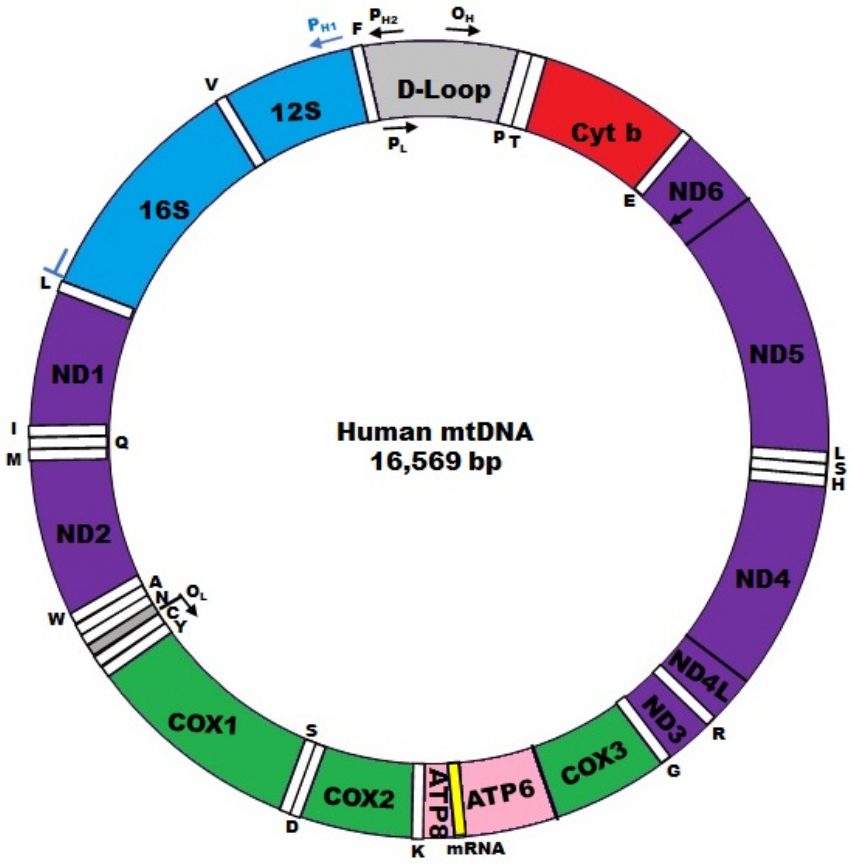

Figure 2. 2 Illustration of the structure of mitochondrial DNA. Mitochondrial DNA is located in the mitochondrial matrix, circular, and it contains 37 genes with 16,569 DNA base pairs.

2.2.2.4 Quantification of PCR products

This procedure was performed in a dark room. 5 µL of PCR products were added into a black 96 well plate (E&K Scientific Products inc, USA) containing 95 µL of 1X TE buffer. 100 µL of PicoGreen solution (1:200 dilution with 1X TE buffer) was added to each well. Following loading, the plate containing the mixture was covered with foil and incubated at room temperature for 10 min in a dark room. After incubation, the plate was read by a SynergyTM^2, a fluorescence microplate reader (BioTeK, Winooski, VT, USA) at 485 nm (excitation)/ 528 nm (emission). All the samples were duplicated.

2.2.2.5 Determination of mitochondrial DNA content analysis using quantitative PCR

The mitochondrial DNA content for all the samples was evaluated using a small size (83 bp) of mtDNA single-copy gene (*D-loop*), and small size (93 bp) of the amplicon of the nuclear single-copy gene (*β2M*) (Table 2) was amplified using real-time quantitative PCR method after modification and optimization of the PCR condition. The mitochondrial and nuclear DNA were amplified using Maxima SYBR Green qPCR Master Mix (2X) and QuantStudio 3 (Applied Biosystems, USA). By using Ct, the relative amplification of mtDNA content ($2^{-\Delta\Delta}$Ct) was calculated.

Table 3 Primers and PCR conditions for mitochondria copy number analysis

Primer	Sequence 5'-3'	Amplicon size (bp)	Annealing temperature (°C)	PCR cycles
mtDNA(D-loop)-Forward	5'-GAT TTG GGT ACC ACC CAA GTA TTG-3'	83	65	30
mtDNA(D-loop)-Reverse	5' -AAT ATT CAT GGT GGC TGG CAG TA -3'			
nDNA (β2M) Forward	5' -GCT GGG TAG CTC TAA ACA ATG TAT TCA -3'	93	63	30
nDNA (β2M) Reverse	5' -CCA TGR ACT AAC AAA TGT CTA AAA TGG T -3'			

2.2.2.6 Data and statistical analysis

Lesion frequency /10 kb was calculated based on the formula in Table 3. Graphpad Prism 7 (Graphpad, San Diego, CA, USA) was used to plot the data and perform statistical analyses.

Table 4 The equation for the calculation of lesion frequency/10 kilobases

Lesion frequency/ 10 kb

1. $sample - blank = blank - corrected\ fluorescence\ value\ (BC)$
2. $Average\ of\ undamaged\ samples's\ BC$
3. $\frac{Each\ sample's\ blank-corrected\ \ fluorescence\ \ value}{Average\ \ blank\ -corrected\ \ fluorescence} = ratio$
4. $negative\ log(-ln) of\ ratio * \frac{10}{Primer\ \ size\ (kb)}$

Chapter-specific methods

2.3 Development, optimization, and evaluation of methods for assessing DNA damage

2.3.1 Cell culture conditions and treatment

HaCaTs were cultured following the conditions in section 2.1.1.1 prior to performing the UV irradiation and H_2O_2 treatment (see section 2.1.2). After irradiation or other treatment, cells were prepared for the alkaline comet assay (see section 2.2.1.1).

2.3.2 Optimization of lysis duration during the comet assay on levels of DNA damage

After treatment with 50 μM H_2O_2, cells were embedded in the 1 % agarose pre-coated slides following the standard alkaline comet assay protocol. The slides were then transferred to the slides transfer rack and lysed at 4 ℃ or room temperature for different incubation duration (30 min, 1 h, 2 h, 4 h or overnight) in lysis buffer with 1% Triton X-100. After each time point of lysis, slides were washed, electrophoresed, neutralized, stained, and washed following the standard alkaline comet assay protocol above.

2.3.3 Evaluation of the effect of including DMSO in lysis buffer of the comet assay on levels of DNA damage

After HaCaTs were irradiated with 0.5 J/cm^2 UVB, on ice, cells were embedded in the 1 % agarose pre-coated slides. The lysis buffer was prepared based on the standard alkaline protocol mentioned in section 2.2.1.2. After the lysis buffer was prepared, 10 % DMSO was added into the lysis buffer. Slides were incubated with 10 % DMSO containing buffer or not with different durations (1 h or overnight) at 4 ˚C. After the lysis step, the rest of the comet assay steps were performed using the standard alkaline comet assay conditions.

2.3.4 Effect of electrophoresis voltage and duration on the detection of nuclear DNA damage.

After each treatment (UVA, UVB, or H_2O_2), comet slides were prepared following the comet assay standard protocol above. After overnight lysis, cells were allowed for 20 min in electrophoresis buffer (300 mM NaOH, 1 mM Na_2EDTA, and pH≥13). In order to optimize the electrophoresis conditions, the experiment was run for 10 or 20 min with different voltages (21 V, 23 V, or 25 V), and the current was allowed to be adjusted automatically by the power supply. After electrophoresis, all the remaining comet procedures performed following the standard comet assay protocol in section 2.2.1.2.

2.3.5 Evaluation of airdrying slides for different durations between neutralization and staining.

After 0.35 J/cm^2 UVB irradiation, all the standard comet assay procedure was performed until the comet slide wash step after neutralization. Slides were then dried for the different duration (1, 2, 3 h or overnight) before staining or straightly stained without drying step. After staining with 2.5 µg/mL of propidium iodide, slides were dried before data analysis.

2.3.6 Evaluation of the effect of ambient vs. subdued illumination on the results from the alkaline comet assay.

Cells with or without UVB irradiation (0.35 or 0.7 J/cm^2) was mixed with 0.6 % LMP agarose and loaded into 1 % pre-coated agarose either with light or without light (in a dark room). All the steps from sample loading, lysis, electrophoresis (25 V for 20 min), neutralization was performed either with ambient light or without light (in a dark room). After the washing step after neutralization, staining with 2.5 µg/mL of propidium iodide was performed in a dark room to avoid the light exposure, and slides were dried at 37 °C incubator overnight before data analysis using Comet IV.

2.3.7 Optimization of blocking buffer solution and secondary antibody concentration in ELISA

The plate was washed three times with PBS (150 µL) and blocked with 4 % milk or 4 % BSA for 1 h at 37 °C in a humidified incubator. The plate was washed with PBS three times. Then the plate was washed with 250 µL of 0.05 % Tween 20 (Fisher, Hampton, NH, USA) in PBS, and 50 µL of different concentrations (0.2, 0.1, 0.05, 0.025, 0.0125, 0.006 or 0.003 µg/mL) of secondary antibody (Rat anti-Mouse IgG1 Secondary Antibody, HRP; eBioscience™, San Diego, CA USA) in 4 % BSA or 4 % milk was added to the well and incubated for 1 h. After incubation, the plate was rewashed with 0.05 % Tween 20 in PBS, and 100 µL of tetramethylbenzidine substrate (TMB; Sigma, St. Louis, MO, USA) was added and incubated for 15 min at room temperature. ELISA stop solution was added, and the plate was read at 450 nm using an EPOCH microplate reader (BioTeK, Winooski, VT, USA).

2.3.8 Data analysis

Graphpad Prism software version 6.07 (Graphpad, San Diego, CA, USA) was used to plot the data and statistical analysis by the Kruskal-Wallis test with Dunn's multiple comparison test and Mann-Whitney tests for the significance ($P < 0.05$). For the experiments with less than triplicates, no statistical analyses were performed.

2.4 Investigation of the formation and repair of UV-induced, bulky adducts in the nuclear and mitochondrial genomes.

2.4.1 Cell culture conditions and treatment

HaCaTs were cultured using the conditions mentioned in section 2.1.1.1.

At 80 % confluency, cells were irradiated with SSR, UVC, and UVB doses (see the calculation in section 2.1.2.1). Prior to performing irradiation, cells were seeded in Petri dishes and grown for 24 h. After two washes with PBS, cells were irradiated with the SSR, UVC, and UVB in PBS, adherent, on ice without a lid. After removing the PBS, Cells were washed twice with PBS. The complete medium was re-introduced to the cells and transferred to a humidified incubator (37 °C and 5 % CO2) and allowed to repair for the different duration (0, 3, 6, 24, or 48 h). Each time point, the media was removed, and cells were washed with PBS. Cells were trypsinized with 0.25 % Trypsin EDTA (Gibco, Waltham, MA, USA) for 10 min at a humidified incubator (37 °C, in a 5 % CO2). Cells were then collected and transferred into microcentrifuge tubes. Centrifugation was performed at 300 x g for 5 min. The cell pellets were frozen at -20 °C before DNA extraction.

2.4.2 DNA extraction and pre-quantification for detection of mitochondrial DNA damage by PCR

DNA extraction was performed using QIamp DNA mini kit (Qiagen, Manchester, UK) and quantified using a NanoDrop One (Thermo Fisher, Waltham, MA, USA) prior to quantitative PCR analysis as described in section 2.2.2 and ELISA.

2.4.3 Mapping of mtDNA damage - Damaged DNA immunoprecipitation sequencing (DDIP-seq)

DDIP-seq is a method to map DNA damage to locations within the genome. The procedures described in section 2.4.3.1 – 2.4.3.3 were performed by Dr. Alaa S. Alhegaili to study the distribution of damage within the nuclear genome. A subsequent, additional analysis described here, was to extend the previous work and specifically identify the location of CPD in the mitochondrial genome.

2.4.3.1 DNA extraction and preparation

After CPD was induced by irradiation, HaCaTs were harvested and centrifuged at 300 xg for 5 min. The cell pellet was washed with PBS twice and resuspended with 10 mL of PBS. After the washing step, cells were centrifuged at 500 xg for 5 min at 4 ˚C. The pellet was resuspended in 500 µL of complete Gen DNA digestion buffer (5 µL of 200 X proteinase K added to 1 mL of Gen DNA Digestion buffer) and incubated at 50 ˚C for 18 h in a shaker. DNA was extracted by Gen DNA module buffers (Diagenode MeDIP kit. Diagenode, Liege, Belgium), using the manufacturer's protocol. After DNA was prepared, DNA was sheared by sonication (Soniprep 150, MSE, London, UK) to obtain 100-300 bp fragments, and 1 % agarose gel electrophoresis was used to confirm the size of DNA fragments.

2.4.3.2. DDIP-seq (damaged DNA immunoprecipitation and next-generation sequencing preparation)

By using an anti-thymine dimer antibody (clone KTM53, Kamiya Biomedical Co, Tukwila, WA) with DNA: antibody ratio (1:1 µg/mL), immunoprecipitation was performed to isolate the CPD-containing fragments. DDIP procedure was followed by the MagMeDIP

kit protocol. DNA was purified and eluted using the QIAquick® PCR purification kit (Qiagen, Manchester, UK). Concentrations for the purified samples were measured with Qubit® fluorimeter using a Qubit® dsDNA HS Assay Kit (Thermo Fisher, Altrincham, UK). After immunoprecipitation, CPD adducts on samples were removed using the PreCR DNA repair kit (New England Biolabs. City, UK) to prevent blocking during PCR amplification steps. After the removal of CPD adducts, DNA samples were amplified using the PCR condition below (Table 4). After qPCR, DNA was purified by Qiaquick PCR purification kit (Qiagen, Manchester, UK) and eluted with elution buffer (Qiagen, Manchester, UK). The MicroPlex Library Preparation Kit (DIagenode, Liege, Belgium) was used to prepare the sequencing for Next-Generation sequencing according to the manufacturer's protocol. The MicroPlex Libraries were purified and quantified by qPCR using the AMPure® XP beads (Beckman Coulter, High Wycombe, UK) and KAPA Biosystems library quantification kit (Roche Diagnostics, Burgess Hill, UK).

Table 5 qPCR conditions after removal of CPD adducts from samples by PreCR DNA repair kit

	Initial denaturation	Denaturation	Annealing	Extension	PCR cycles
Temperature (°C)	95	95	65	72	25
Time	2 min	10 sec	30 sec	1 min	

2.4.3.3 Bioinformatic analysis for NGS

Raw data output from Illumina next-generation sequencer was generated in fastq data format through the bcl2fastq program. After the fastq data was generated, quality control

was performed using TQC. Downstream analysis was performed to remove and align the fastq data to the reference genome by using the Trimmomatic and the mapping program, Burrow-Wheeler Aligner (BWA). After alignment, each sample was mapped to the genome assembly GRCh38. A SAM file, which is a format used to map sequences, was generated by using SAMtools to verify the specific information about the location of the gene of interest in the genome. Finally, the Integrative Genomics Viewer was used to visualize the mapped data using the reference genome GRCh38. After mapping, the functional consequence of CPD was identified using the GENCODE tool.

2.4.3.4 Evaluation of the specificity of the anti- T<>T by ELISA

Double-stranded and single-stranded DNA (50 µg/mL; 50 µL/well) exposed to UVC or H_2O_2 were added to the DNA-bind 96 well plates (Corning™, Corning, NY, USA) and incubated in a humidified incubator for 1 h. Following incubation, the plate was washed three times with 150 µL of PBS, and then the plate was blocked with 4 % BSA in PBS for 1h at 37 °C in a humidified incubator. The plate was washed with PBS three times. 50 µL of different concentrations (0.125, 0.25, 0,5 or 1 µg/mL) of Anti-Thymine Dimer (as used in DDIP) in blocking buffer (4% BSA) was added to the well and incubated for 1 h. The plate was washed with 250 µL of 0.05 % Tween 20 in PBS, and 50 µL of 1: 10,000 dilution (0.05 µg/mL, final concentration) of secondary antibody (Rat anti-Mouse IgG1 Secondary Antibody, HRP) in 4% BSA was added to the wells and incubated for 1 h. After incubation, the plate was rewashed with 0.05 % Tween 20 in PBS, and 100 µL of TMB substrate was added and incubated for 15 min at room temperature. After 15 min of incubation, the ELISA stop solution was added, and the plate was read at 450 nm using an EPOCH microplate reader.

2.4.4 Quantification of mtDNA damage

To validate the mitochondrial CPD data noted by DDIP-seq, short-range PCR of mtDNA damage in HaCaTs induced by UVB or UVC irradiation was performed. The PCR was performed (see the details in section 2.2.2.3). PCR products were quantified using PicoGreen fluorescence (details in section 2.2.2.4). Lesion frequency/10 kb was calculated according to the formula in Table 3.

2.4.5 Quantification of mtDNA content

To evaluate the mitochondrial DNA content, quantification of mtDNA content analysis was performed using qPCR. The PCR conditions were followed in section 2.2.2.5. After PCR, the relative amplification of mtDNA was calculated using the $2^{-\Delta\Delta}$.

2.4.6 Statistical analysis

All experiments were triplicated and expressed as mean ±SEM. A one-way analysis of variance (ANOVA) test was performed for statistical analysis using GraphPad Prism software v.6.0. Significance was set at $P < 0.05$.

2.5 Investigation of the effect of chronic bacterial infection on nuclear DNA damage and repair

2.5.1 Cell culture conditions

BE-M17 (infected and uninfected cells) were cultured separately as a monolayer in cell culture flasks in Dulbecco's modified Eagle's medium (Gibco, Waltham, MA, USA) supplemented with 10% fetal bovine serum (Gibco, Waltham, MA, USA), without antibiotics, at 37 °C, in a 5% CO_2 humidified incubator. Confirmation of Mycoplasma infection was achieved, as described in section 2.1.1.2.

2.5.2 Cell treatment and preparations

Hydrogen peroxide treatment was used to induce DNA damage (SB/ALS and oxidized purines) in both infected and uninfected BE-M17 cells. After two washes with PBS, the cells were exposed to freshly prepared 50 μM H_2O_2 for 30 min, on ice. After treatment, the cells were washed with PBS, complete medium re-introduced, and the cells transferred to a humidified incubator (37 °C, 5 % CO_2). The cells were then allowed to repair for different durations (0 min, 30 min, 2 h, 6 h, or 24 h). At each time point, batches of cells were removed from the incubator, the medium removed, and the cells washed with PBS. Cells were trypsinized with 0.25 % Trypsin EDTA for 1 min at room temperature, prior to centrifugation (7000 x g for 5 min), and resuspension in PBS. The cells were then counted, and the required number transferred to the comet assay.

2.5.3 Alkaline and hOGG1-modified comet assay

The alkaline and enzyme-modified comet assays were performed as described elsewhere (section 2.2.1.2). Briefly, 80 μL of 0.6 % low melting agarose gel, containing ~12,000 cells, were added to pre-chilled, pre-coated microscope slides, and left to solidify under a

coverslip on a chilling plate. The coverslips were then removed, and the slides incubated in a lysis buffer containing 1 % Triton X at 4 °C overnight. Human 8-oxoguanine DNA glycosylase-1 (hOGG1; New England Biolabs, Ipswich, MA, USA) treatment was performed prior to the electrophoresis step. Slides were washed for 20 min with ice-cold ddH_2O and incubated, either with enzyme reaction buffer (ERB; 40 mM HEPES, 0.1 M KCl, 0.5 mM Na_2EDTA, 0.2 mg/mL BSA with pH 8) or with ERB containing 60 µL of 3.2 U/mL hOGG1. Each gel was then covered with a coverslip and incubated for 1 h at 37 °C. After hOGG1/ERB treatment, slides were placed in COMPAC50 slide racks and transferred to a COMPAC50 electrophoresis tank containing electrophoresis buffer. Following incubation for 20 min, electrophoresis was performed (1.19 V/cm) for 20 min. The slide-containing racks were then transferred sequentially to tanks containing neutralization buffer; cold ddH_2O (20 min); propidium iodide (2.5 µg/mL) for 20 min in the dark, i.e., with tank lid closed; and finally washed in cold ddH_2O (20 min). After the final wash, the slides were dried before the analysis of comets using Comet IV software.

2.5.4 Data analysis

The data from the comet assay were plotted using Graphpad Prism software v.6.0.

CHAPTER 3

Development, optimization, and evaluation of methods for assessing DNA damage

This chapter has been partially published:

Mahsa Karbaschi, Yunhee Ji, Abdulhadi Mohammed S Abdulwahed, Alhanoof Alohaly, Juan F Bedoya, Shanna L Burke, Thomas M Boulos, Helen G Tempest, Marcus S Cooke

Evaluation of the Major Steps in the Conventional Protocol for the Alkaline Comet Assay

International Journal of Molecular Sciences. 2019

Volume 20 (23), 6072 pages

https://doi.org/10.3390/ijms20236072

Overview of Chapter 3

This chapter includes the results of the optimization of the methods used in this thesis. Many of the methods detailed in this thesis have followed the manufacturer's protocol or descriptions from the references in the literature. However, some optimization and development of methods were needed to maximize the efficiency, reliability, and sensitivity of the assays, particularly if cell-type-specific modifications were required. First, in this chapter, the major steps of comet assay were evaluated to determine whether all the steps are necessary to be performed without altering the levels of DNA damage using HaCaT cells with different DNA damaging agents to induce DNA damage (H_2O_2 or UV irradiation) as a model system. Secondly, the annealing temperature for the primers used in the mitochondrial copy number analysis using quantitative PCR methods was optimized to increase the efficiency of the assay. The third part of this chapter is the optimization of ELISA (blocking solution and secondary antibody) to assess the detection of CPD in DNA.

3.1 Alkaline comet assay

The alkaline comet assay is one of the most sensitive methods to detect nuclear DNA damage in individual cells. This method is very sensitive and has many benefits (e.g., low cost and ease of use). However, because of the duration of running the assay and many steps in a dark environment, it can pose challenges for researchers performing the assay. In this section, alkaline comet assay steps were re-evaluated to minimize the duration of the protocol and evaluate and whether all the steps are necessary while ensuring the quality data from the assay is maintained.

Aim

This section aims to evaluate the critical steps of comet assay to simplify the assay, to minimize the duration of the assay, and increase the quality of the assay to detect DNA damage in the cells.

Results

3.1.1 Optimization of lysis conditions for the detection of nuclear DNA damage (SB/ALS)

The effect on the detection of DNA damage of lysis duration and temperature at which lysis is performed during the comet assay was evaluated to minimize the duration of lysis. Different durations of lysis (30 min, 1, 2, 4, or overnight) at temperature (room temperature and 4 °C) were investigated. Additionally, the effect of lysis buffer containing DMSO in HaCaTs was evaluated to optimize the condition for the lysis buffer. The inclusion of DMSO has been shown previously to protect white blood cells and lymphocytes from free radicals as a scavenger during the lysis step of the comet assay [69].

3.1.1.1 Evaluation of the effect of lysis duration during comet assay on levels of DNA damage

HaCaTs and H_2O_2 were used as a representative cell line and DNA damaging agent, respectively. Following incubation with 50 μM H_2O_2, processing cells using the standard alkaline comet assay conditions (overnight lysis at 4 °C), resulted in a %TD of approximately 38.095 %TD (Figure 3.1.1). Lysis at room temperature in all different durations (30 min, 1, 2, 4 h or overnight) did not show any significant difference compared with lysis overnight at 4 °C. However, both cells untreated or treated with 50 μM H_2O_2 and lysed for 30 min at 4 °C showed significantly different levels of DNA damage ($P<0.01$

or P<0.0001) when compared with overnight lysis at 4 °C. Although mean levels of damage appeared higher (e.g., 40.33 %TD), performing lysis at room temperature did not significantly alter the level of nuclear DNA damage detected, compared to the standard conditions (Figure 3.1), demonstrating that lysis can be successfully performed in as little as 30 min, at room temperature, decreasing the overall assay run time.

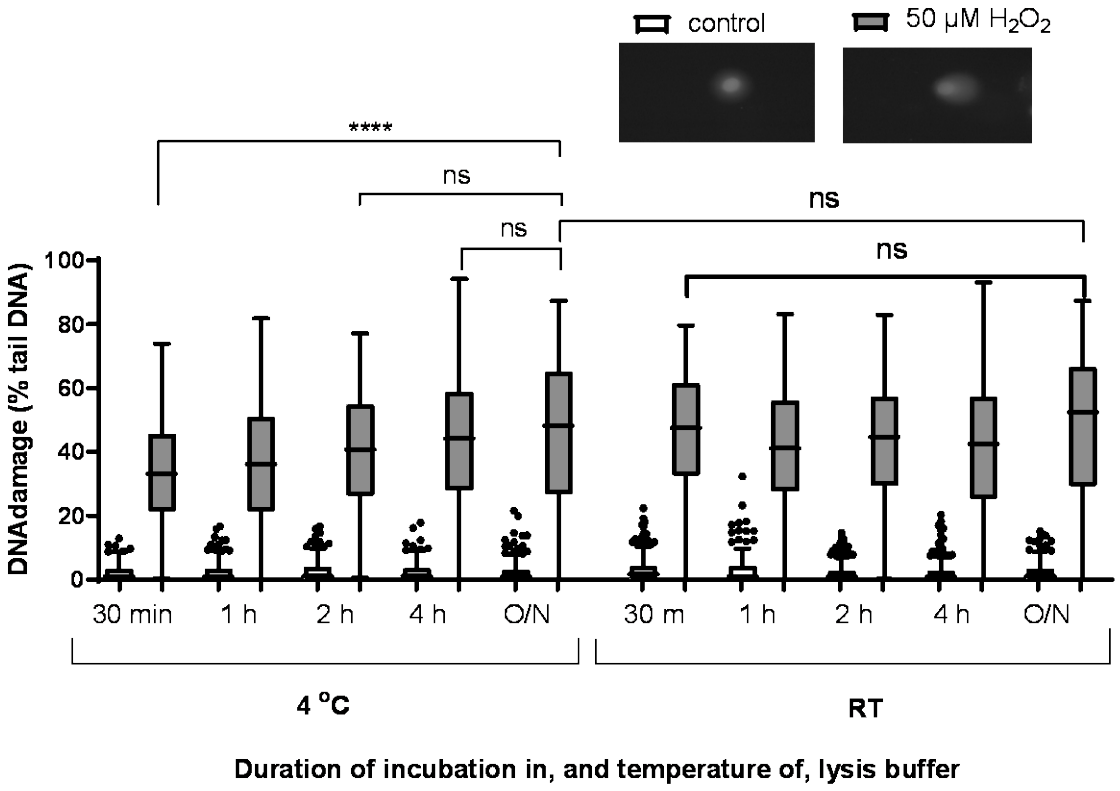

Figure 3. 1 Lysis for 30 min at room temperature is as effective as overnight at 4 °C. HaCaTs were treated with 50 µM H_2O_2. The slides were then incubated in lysis buffer for different durations of time at 4 °C or room temperature (RT). Tukey box and whiskers plots were from three independent experiments, 100 determinations per experiment. (O/N: Overnight, P>0.05, Mann-Whitney test). ** represents P<0.01, and **** represents P<0.0001.

3.1.1.2 Evaluation of the effect of DMSO in lysis buffer on levels of DNA damage.

DMSO has been shown previously to protect white blood cells and lymphocytes from radicals as a scavenger during the lysis step of the comet assay. However, lysis buffer containing 10 % DMSO did not decrease levels of DNA damage in the form of SB and ALS significantly for the irradiated with 0.5 J/cm^{2}UVB or sham irradiated HaCaTs with the following lysis condition (1 h lysis at room temperature) when compared to without DMSO-containing buffers. However, the levels of DNA damage were decreased in HaCaTs irradiated with 0.5 J/cm^{2}UVB and lysed with 10 % DMSO containing buffer (29.5 %TD) when compared with the cells lysed overnight lysis at 4 °C (31.6 %TD). Still, it was not statistically significantly different (Figure 3.2). These results demonstrated that the lysis buffer containing 10 % DMSO did not affect the levels of DNA damage in HaCaTs following UVB exposure.

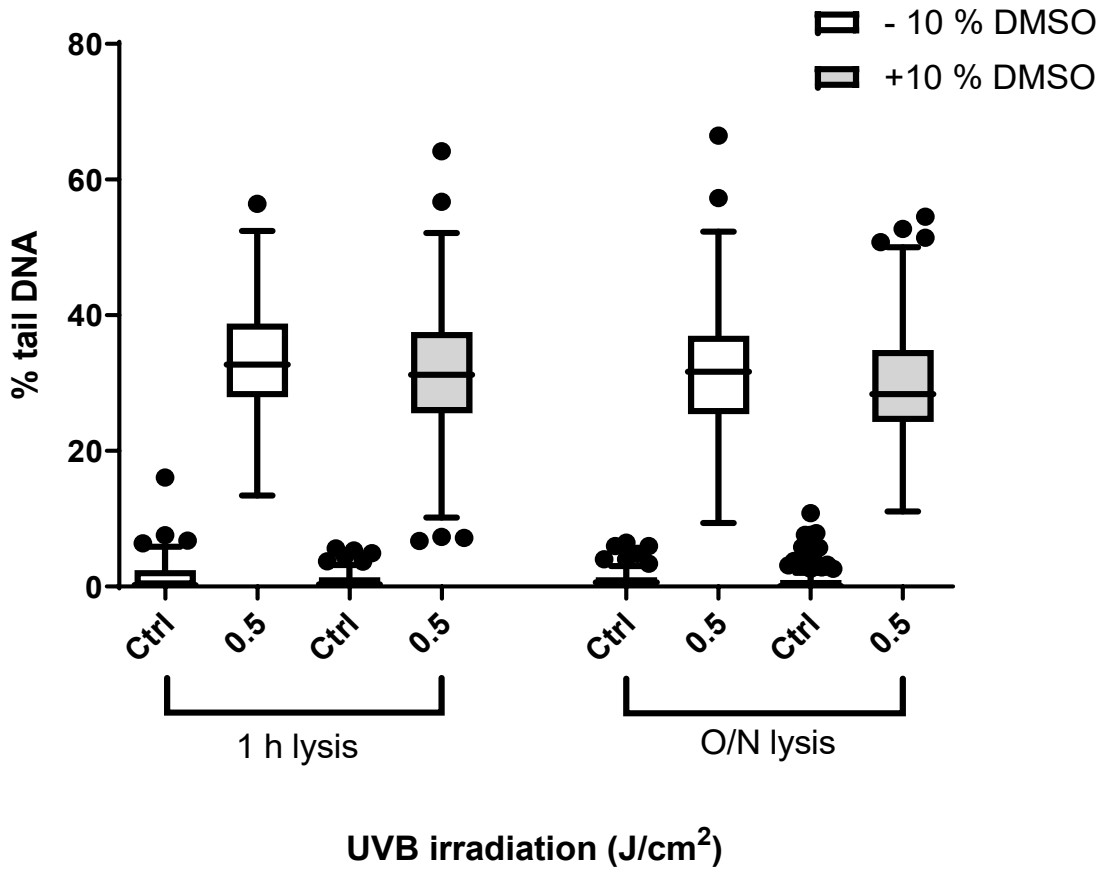

Figure 3. 2 10 % DMSO in lysis buffer did not decrease the levels of DNA damage in HaCaTs. HaCaTs were irradiated with 0.5 J/cm^2 UVB, on ice, prior to performing the comet assay. Different durations of lysis (1 h or overnight) and a lysis buffer containing with or without 10 % DMSO were shown. Tukey box and whisker plot of median and IQR from two individual experiments of 100 determinations per experiment.

3.1.2 Effect of electrophoresis voltage and duration on the detection of nuclear DNA damage.

One of the main steps of alkaline comet assay is the electrophoresis step. The alkaline condition of electrophoresis buffer relaxes the packed nucleoid body by removing the DNA scaffold and denatures the double-stranded DNA to single-stranded DNA. During electrophoresis, damaged DNA in the form of SSB/ALS will be pulled out by the current and voltage. Therefore, this step allows each comet to form tails if DNA damage is present. Therefore, the optimization of the electrophoresis step is important to increase the efficiency of the assay to evaluate DNA damage using the comet assay. For optimizing the electrophoresis step, HaCaTs and UVB, UVA, and H_2O_2 were used as a representative cell line, and DNA damaging agents, respectively. The results showed that the baseline of DNA damage in untreated HaCaTs using 25 V had higher % TD (UVA; 6.32, UVB; 7.53 and H_2O_2; 6.32 %TD) than other voltages (less than 5 %TD). In addition, the data showed that increasing the voltage of electrophoresis formed a larger tail of comets in HaCaTs irradiated with UVA, UVB, or treated with H_2O_2. However, 25 V provided the condition to pull out the most damaged DNA in HaCaTs irradiated UVA, UVB, or treated with H_2O_2, and it also showed linear dose-response (Figure 3.3). From these results, 25 V showed the optimal voltage condition to detect DNA damage in the alkaline comet assay. Following the optimization of electrophoresis voltage, the duration of electrophoresis was studied. After assessing the optimal voltage, 25 V was selected as it produced comparable results from the experiment performed in reference [70], and electrophoresis duration was tested. Electrophoresis for 20 min showed higher DNA damage (7.53 %TD) compared with 10 min (3.14 %TD) in sham irradiated HaCaTs. In addition, HaCaTs irradiated with 0.5 or 1 J/cm^2 UVB showed greater DNA damage pulled out in 20 min (27.33 or 41.63 %TD) than

10 min (17.16 or 23.04 %TD). Furthermore, 20 min showed a linear dose-response (Figure 3.4). The results demonstrated that 20 min is the efficient duration to form the tail in the electrophoresis run at 25 V.

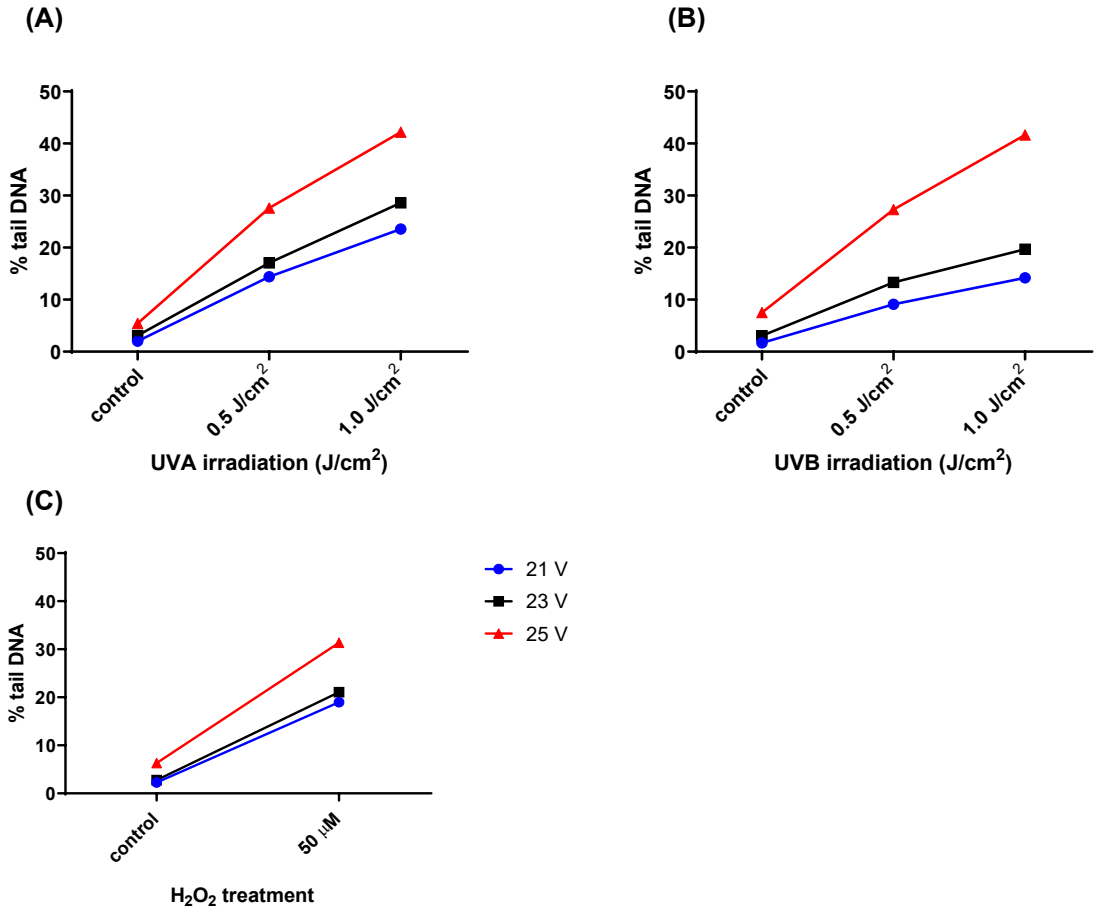

Figure 3. 3 Electrophoresis performed at 25 V provides optimal detection of DNA damage in the alkaline comet assay. HaCaTs were irradiated with (A) UVA (5 or 10 J/cm^2), (B) UVB (0.5 or 1 J/cm^2) or treated with (C) 50 µM H_2O_2 prior to the alkaline comet assay being performed with the electrophoresis voltage at 21, 23, or 25 V. Data represent the mean of 200 determinations from n=2 individual experiments.

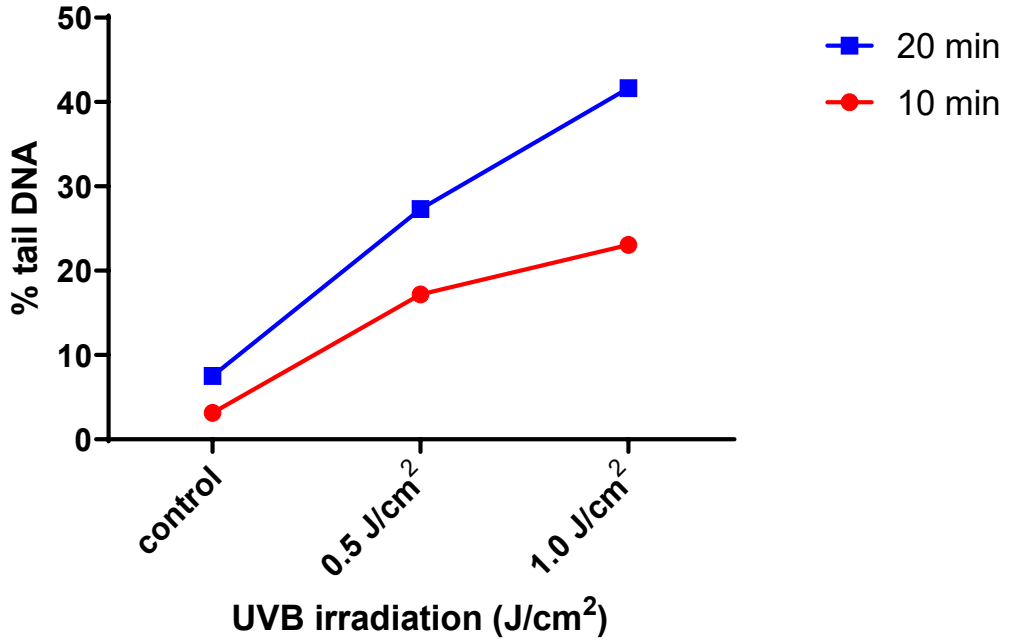

Figure 3. 4 Performing electrophoresis for 20 min reveals greater DNA damage than for 10 min, in the alkaline comet assay. Cells were irradiated, on ice, with 0.5 or 1 J/cm^2 UVB prior to performing the comet assay. Electrophoresis was performed at the previously optimized voltage, 25 V (see Figure 3.3) for either 10- or 20-min. Data represent the mean of 200 determinations from n=2 individual experiments.

3.1.3 Evaluation of air-drying slides for different durations between neutralization and staining.

The drying step following the neutralization step is one of the longest durations of the comet assay. Since the protocol of the conventional alkaline comet assay is overnight drying and rehydrating after drying prior to the staining step, minimizing the duration of the drying step will help to reduce the time taken to perform the comet assay. In this section, different durations (0, 1, 2, 3, or overnight) of airdrying slides were evaluated.

For optimizing the airdrying step after neutralization, HaCaTs and UVB were used as a representative cell line and DNA damaging agent, respectively. The results demonstrated that levels of DNA damage for all different duration of drying in the cells irradiated with 0.7 J/cm^2 UVB or sham irradiated were not significantly different. In addition, there was not a significant difference in the 0.35 J/cm^2 UVB irradiated HaCaTs between 1, 2 h, overnight, and undried slides. However, a significant difference was identified in the 0.35 J/cm^2 UVB irradiated HaCaTs between slides dried for 3 h and undried samples with 2.48 %TD differences ($P < 0.01$) (Figure 3.5). These experiments demonstrate that drying slides for 1 h before the staining step of the comet was comparable with the overnight drying in the conventional comet assay, and hence can significantly shorten the duration of the assay.

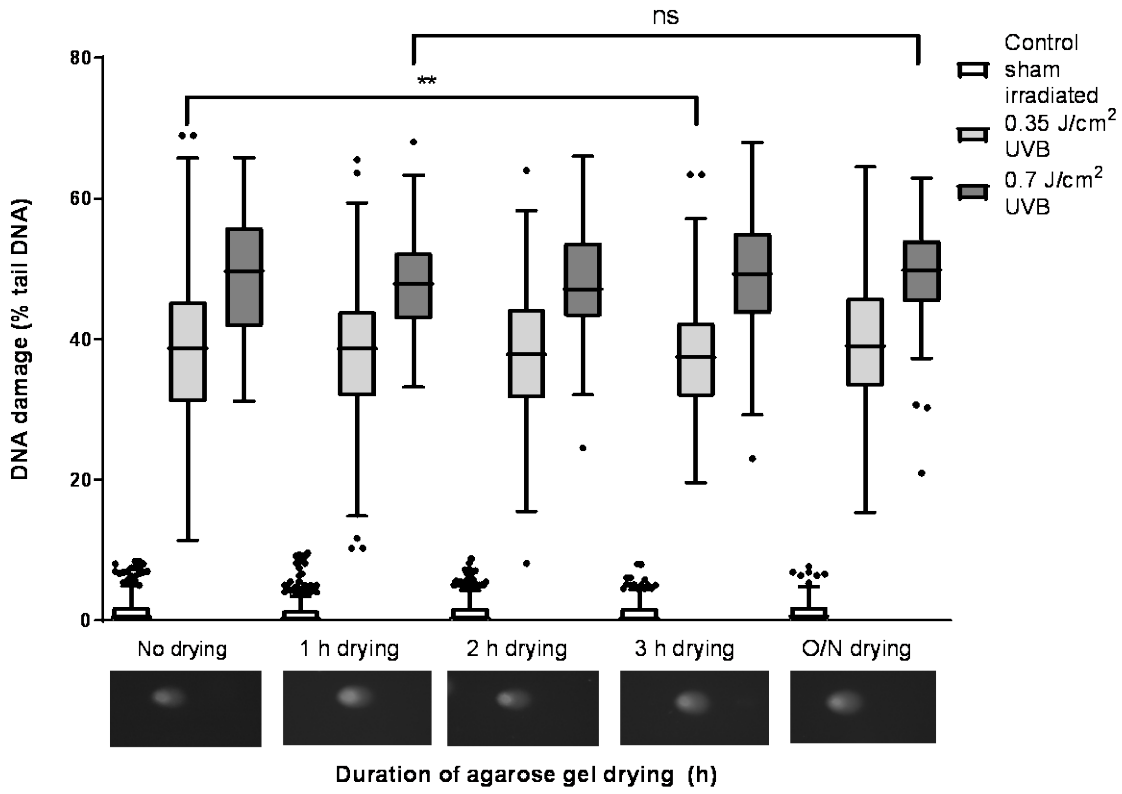

Figure 3. 5 Drying comet assay gels for 1 h is as effective as overnight (O/N), which is the convention. Cells were irradiated with 0.35 or 0.7 J/cm^2 UVB, on ice, as described for the standard alkaline comet assay methods (see section 2.2.1.6.). The gels were then dried for either 0, 1, 2, 3, h or overnight prior to staining. Tukey box and whisker plot of median and IQR of 100 determinations per treatment per experiment. n=2 individual experiments. (** represents P<0.01.)

3.1.4 Evaluation of the effect of ambient vs. subdued illumination on the results from the alkaline comet assay

Conventionally, comet assay is performed under subdued (red) light – the theory being that white light may include artefactual DNA damage. However, there does not appear to be any information in the literature to support this requirement. Performing the comet assay under subdued light conditions requires a dedicated room without light, and the assay can be technically challenging to perform due to low light levels. Therefore, the effect of ambient light on the levels of DNA damage during the comet assay was investigated.

HaCaTs were irradiated with 0.35, 0.7 J/cm^2 UVB, or sham irradiated (covered with foil). The results in Figure 3.6 showed that ambient light did not induce DNA damage sham irradiated HaCaTs. In addition, the 0.35 J/cm ^{2} UVB irradiated samples showed no significant difference in damage between using ambient light (44.67 %TD) and subdued light (45.08 %TD) (Figure 3.6). Furthermore, the cells irradiated with 0.7 J/cm^2 UVB showed no significant effect of ambient light shown in the levels of DNA damage ($P > 0.05$).

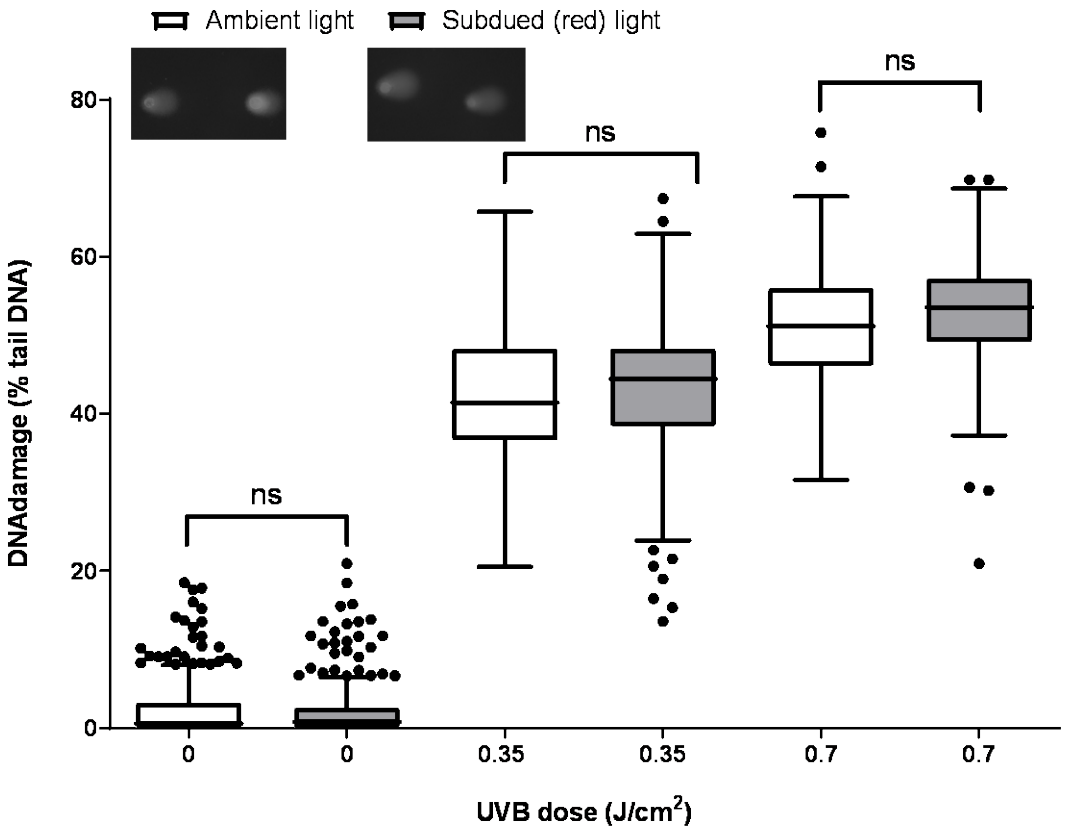

Figure 3. 6 The workup of slides for the ACA under ambient light does not induce adventitious DNA damage. Cells were irradiated with 0.35 or 0.7 J/cm^2 UVB, on ice. Alkaline comet assay was performed as described in chapter 2, section 2.2.1.5. Tukey box and whisker plot of median and IQR of 300 determinations from n=3 individual experiments.

3.1.5 Evaluation of the sensitivity of the comet assay to detect nuclear DNA damage

The sensitivity of the comet assay to measure nuclear DNA damage was evaluated using the dose-response of different sources of DNA damaging agents. UVA showed that increasing doses increased the levels of DNA damage in forms of SB/ALS. The sham irradiated cells showed 5.439 %TD, and 5 and 7 J/cm ^{2} UVA irradiation showed 27.67 %TD and 42.19 %TD (Figure 3.7 A). As shown in Figure 3.7 B, the cells irradiated UVB also showed increased levels of DNA damage by increasing doses of UVB. Sham irradiated cells showed 2.1193 % TD, and it was increased 10.7188 %TD in 0.1 J/cm ^{2}, and the % TD was increased 10-fold in 0.25 J/cm^2 (20.5151 %TD). Levels of DNA damage increased 18-fold in the 0.5 J/cm^2 UVB irradiated cells when compared with sham irradiated cells. The cells irradiated with 0.75 J/cm^2 UVB was increased to 41.36 %TD, but it was only 5 %TD higher than 0.5 J/cm^2 irradiated samples. The highest does of UVB was 1 J/cm^{2,} and it was increased 23 times higher than sham irradiated samples, but it was 6 %TD higher than 0.75 J/cm^2 irradiated samples. The results are shown in Figure 3.7C demonstrates that by increasing the concentration of H_2O_2, the % TD was increased. At 50 µM H_2O_2 treatment, % TD was increased to 30.34 %TD, which is 30-fold higher than cells without treatment. Following 100 µM H_2O_2 treatment, the % TD was 49.405, ~1.6 times higher than 50 µM H_2O_2 treatment. The data showed the linear shape of dose-response until 150 µM H_2O_2 treatment (60.695 %TD), which is 1.2 times higher than 100 µM H_2O_2 treatment. However, the rate of DNA damage levels started to plateau between 150 to 300 µM H_2O_2 treatment (60.695 %TD and 68.935 %TD, respectively).

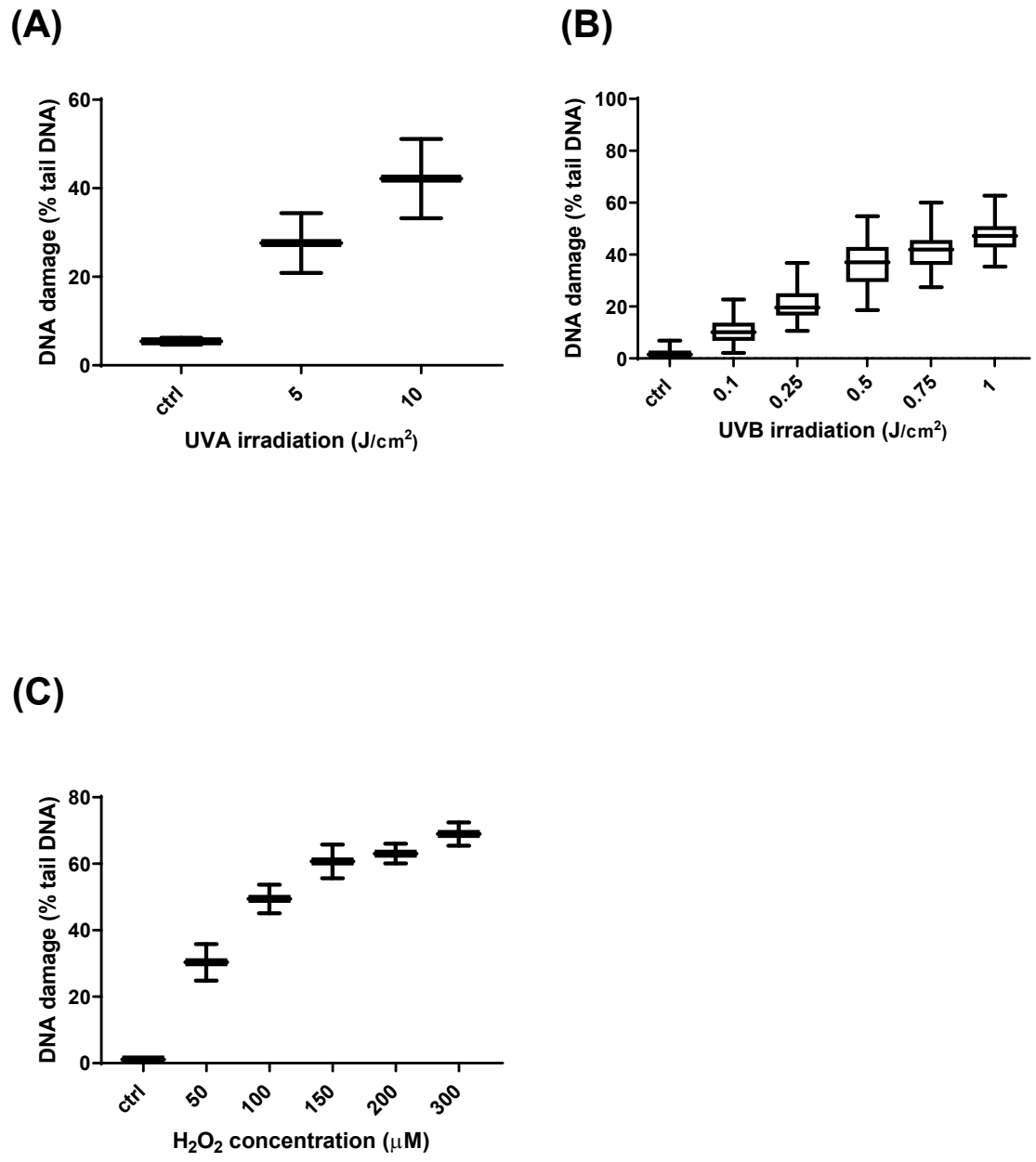

Figure 3. 7 Nuclear DNA damage (SB/ALS) increased with increasing doses of (A) UVA, (B) UVB, or (C) H_2O_2 in HaCaTs. Cells were irradiated with (A) 5 or 10 J/cm^2 UVA, (B) 0.1, 0.25, 0.5, 0.75 or 1 J/cm^2 UVB or (C) 50, 100, 150, 200, or 300 μM H_2O_2, on ice. Alkaline comet assay was performed as described in chapter 2, section 2.2.1.5. Tukey box and whisker plot of median and IQR of 200 determinations from n=2 individual experiments.

3.2 Optimization of mitochondrial copy number analysis

Mitochondrial depletion is a major issue leading to mitochondrial dysfunction, which is one of the factors that play an important role in pathogenesis. Many studies show that mutation, deletions, and changes in mtDNA are associated with many diseases such as cancers, heart, and neurodegenerative diseases. Therefore, the methods which could evaluate mtDNA is important to assess the entire mitochondrial function. Mitochondrial copy number analysis is one of the methods to assess whether mitochondria are healthy or not. In our study in chapter 4, we have used this analysis to confirm that if mtDNA damage was diluted by increasing levels of healthy mtDNA contents in UV induced cells. Therefore, in this section, primers for the mitochondrial copy number analysis were optimized to increase efficiency.

Aim

To determine the optimal annealing temperature of primers for mitochondrial copy number analysis.

Results

3.2.1 Optimization of mitochondrial primers (D-loop lesion) for mitochondrial copy number analysis

The results from the qPCR data of optimization of mitochondrial primers indicated that 65 ˚C of annealing temperature showed the highest efficiency (98.480 %) without any contamination and primer dimers compared with 60 or 63 ˚C (91.097 or 93.912 %) (Figure 3.8). The annealing temperature of 65 ˚C for D-loop lesion primer was chosen for the qPCR experiment for mitochondrial copy number analysis.

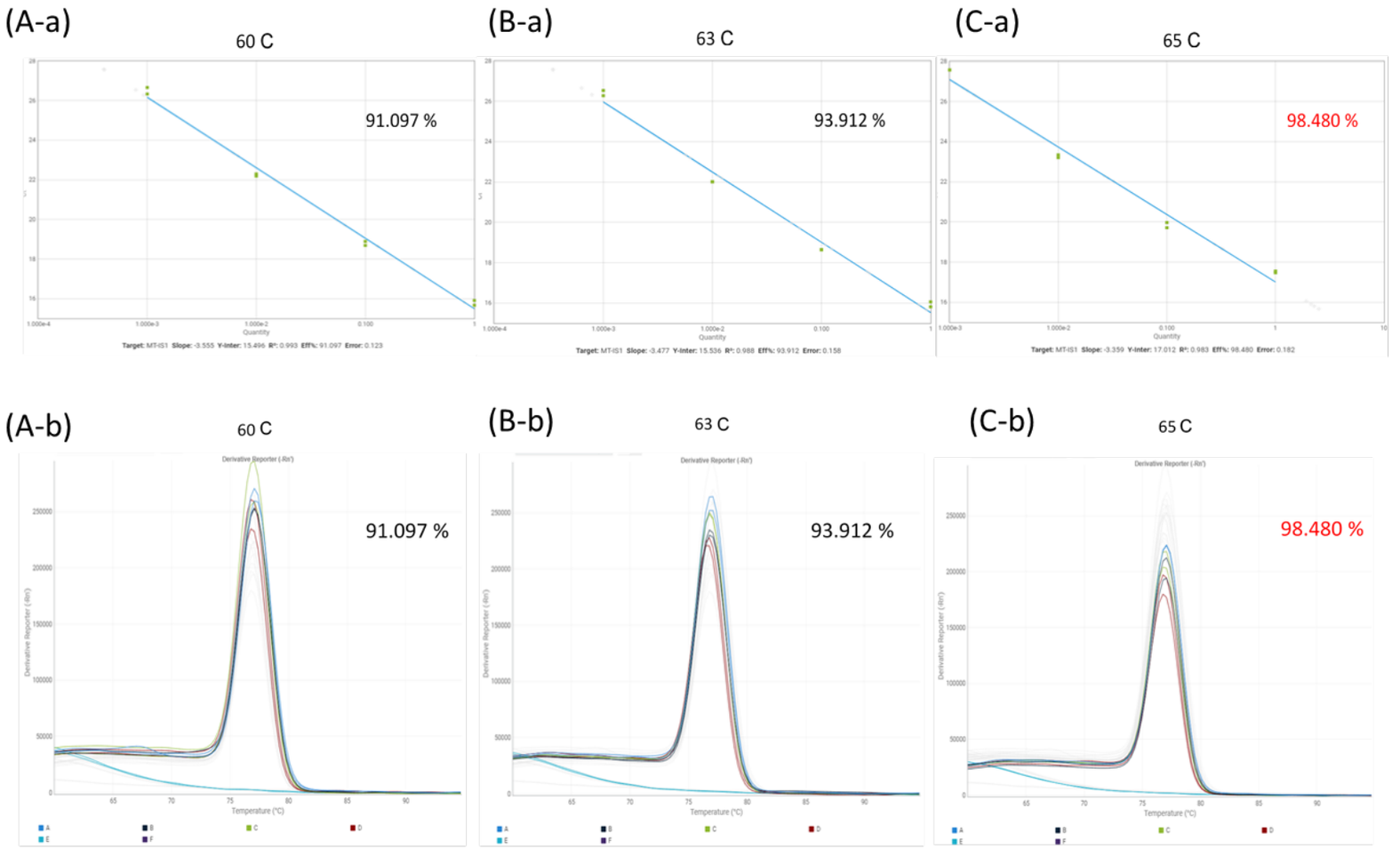

Figure 3. 8 Optimization of annealing temperature (A) 60 (B) 63 or (C) 65 ˚C for PCR primers for the mitochondrial single-copy gene (*D-loop*: 83 bp). 1, 10, 100, or 1000 dilution factors were used to generate the (-a) standard curve or (-b) dissociation curves using the methods described in Chapter 2, Table 2.

3.2.2. Optimization of nuclear single-copy gene (*hB2M*) primers for mitochondrial copy number analysis

As shown in Figure 3.9, the most efficient conditions for the nuclear single-copy gene primer was determined to be with an annealing temperature of 63 ˚C giving a 99.586 % efficiency. The efficiency at 62 ˚C was lower (96.269 %), and 64 ˚C was higher (126 %) than 63 ˚C. The dissociation curves showed that there were no primer-dimers or contamination with all conditions.

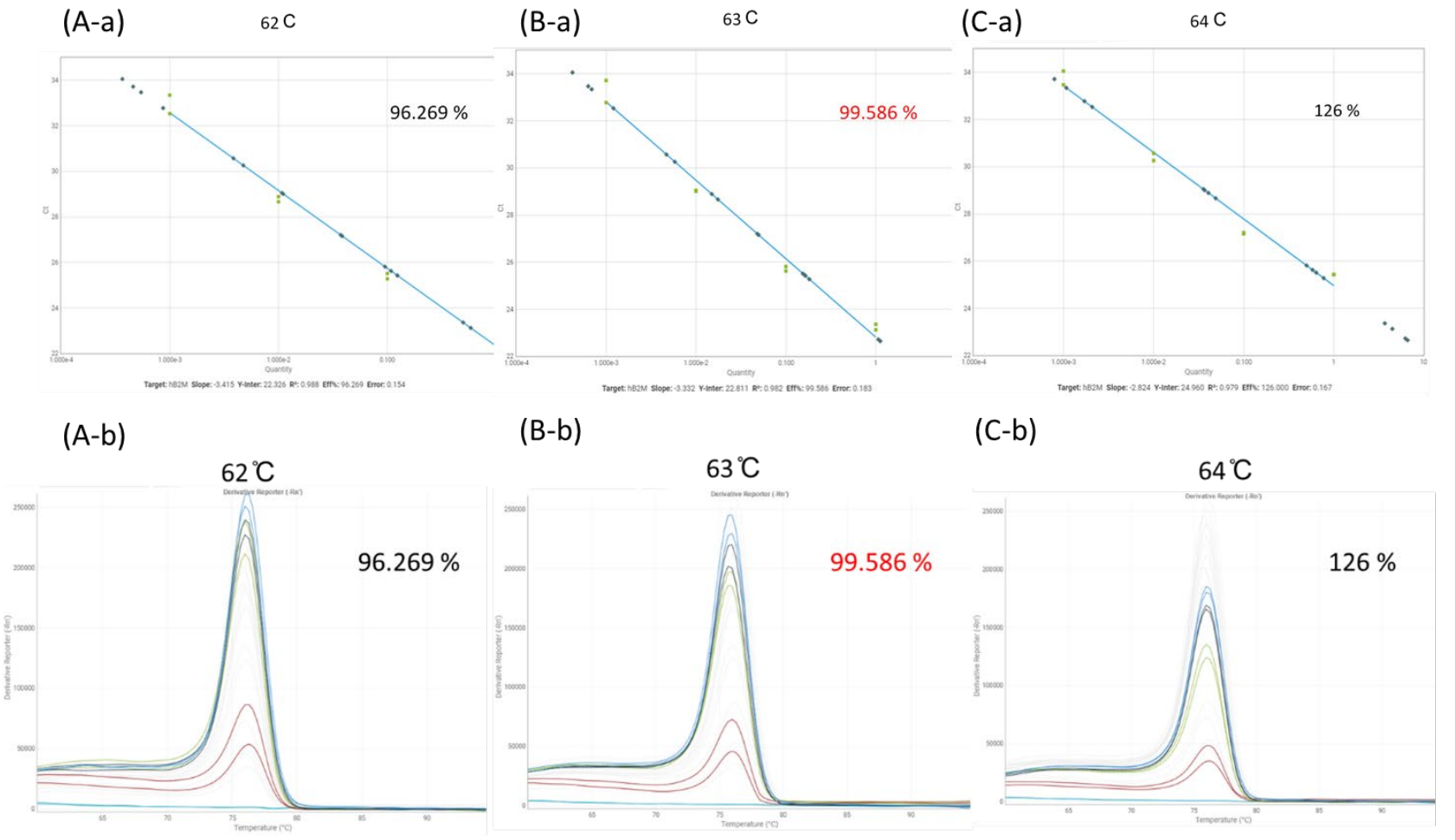

Figure 3. 9 Optimization of annealing temperature (A) 62 (B) 63 or (C) 64 ˚C of PCR for a nuclear single-copy gene (*hB2M*: 93 bp). 1, 10, 100, or 1000 dilution factors were used to generate (-a) standard curve or (-b) dissociation curves using the methods in Chapter 2, Table 2.

3.3 ELISA

ELISA is one of the simplest and most widely used methods to measure the combination of antibodies and antigen. ELISA has been used to detect damaged DNA (e.g., 8-oxodG and T<>T). This part of the present chapter is the optimization of critical parameters in ELISA for the detection of T<>T, in order to further characterize the monoclonal antibody used in DDIP-seq. A previous study indicated that the reported ELISA conditions were sub-optimal, and therefore not sufficient to fully characterize the primary antibody's specificity [71]. This included a high background reading showing non-specific binding of the antibody on the plate and DNA damage product. Therefore, several parameters were examined to increase the efficiency of the assay and allow further characterization of the antibody.

Aim

To optimize the conditions of blocking solution, and primary and secondary antibody concentrations, prior to characterization of the primary antibody specificity (see Chapter 4).

Results

3.3.1 Optimization of blocking buffer solution and secondary antibody concentration

The data showed that at the highest concentration of secondary antibody [0.2 µg/mL (1:2500)] in the absence of DNA on the plate, gave a significant absorbance, indicating that the secondary antibody was binding non-specifically to the plate. The introduction of a 4 % BSA blocking solution resulted in a lower absorbance at 450 nm with the highest concentration of secondary antibody (0.2 µg/mL, 0.071) than a 4 % milk blocking solution (1.256). The blocking solution with 4 % milk also showed absorbance at 450 nm with the lowest concentration of secondary antibody [0.003 µg/mL (1:160000 dilutions), 0.02], and this absorbance was the same as seen with the 4 % BSA buffer at the 1:5000 dilutions [0.1 µg/mL, (0.02)]. The blocking solution with 4 % BSA did not show any absorbance from 1:20000 dilutions (0.025 µg/mL) (Figure 3.10 A). The blocking buffer with 4 % BSA illustrated optimal conditions. The 1:80000 dilution (0.006 µg/mL) of secondary antibody was chosen to be used for ELISA to make sure there was no non-specific binding to the plate in the absence of DNA (Figure 3.10 B).

3.3.2. Optimization of the primary antibody (anti-CPD) concentration

The results in the 3.10 (C) showed that primary antibody concentrations were tested using different dilutions (0.125, 0.25, 0,5 or 1 µg/mL) against double-stranded or single-stranded calf thymus DNA irradiated with 0.12 J/cm^2 UVC. UVC is highly effective at introducing CPD. The results showed that there were no significant differences in absorbance (i.e., binding) between all the concentrations of primary antibody against both double-stranded and single-stranded DNA. The lowest antibody dilution (1:4000, 0.125 µg/mL) was

selected as an optimal condition to decrease the amount of antibody used and, therefore, costs. Interestingly, there was a significant difference in absorbance between double-stranded and single-stranded DNA at all concentrations. Binding to single-stranded DNA gave a higher absorbance at all of the concentrations of primary antibody, compared to double-stranded DNA. For example, at 0.125 μg/mL (1:4000) of primary antibody, single-stranded DNA showed an absorbance of 1.077, whereas double-stranded DNA showed an absorbance of 0.385.

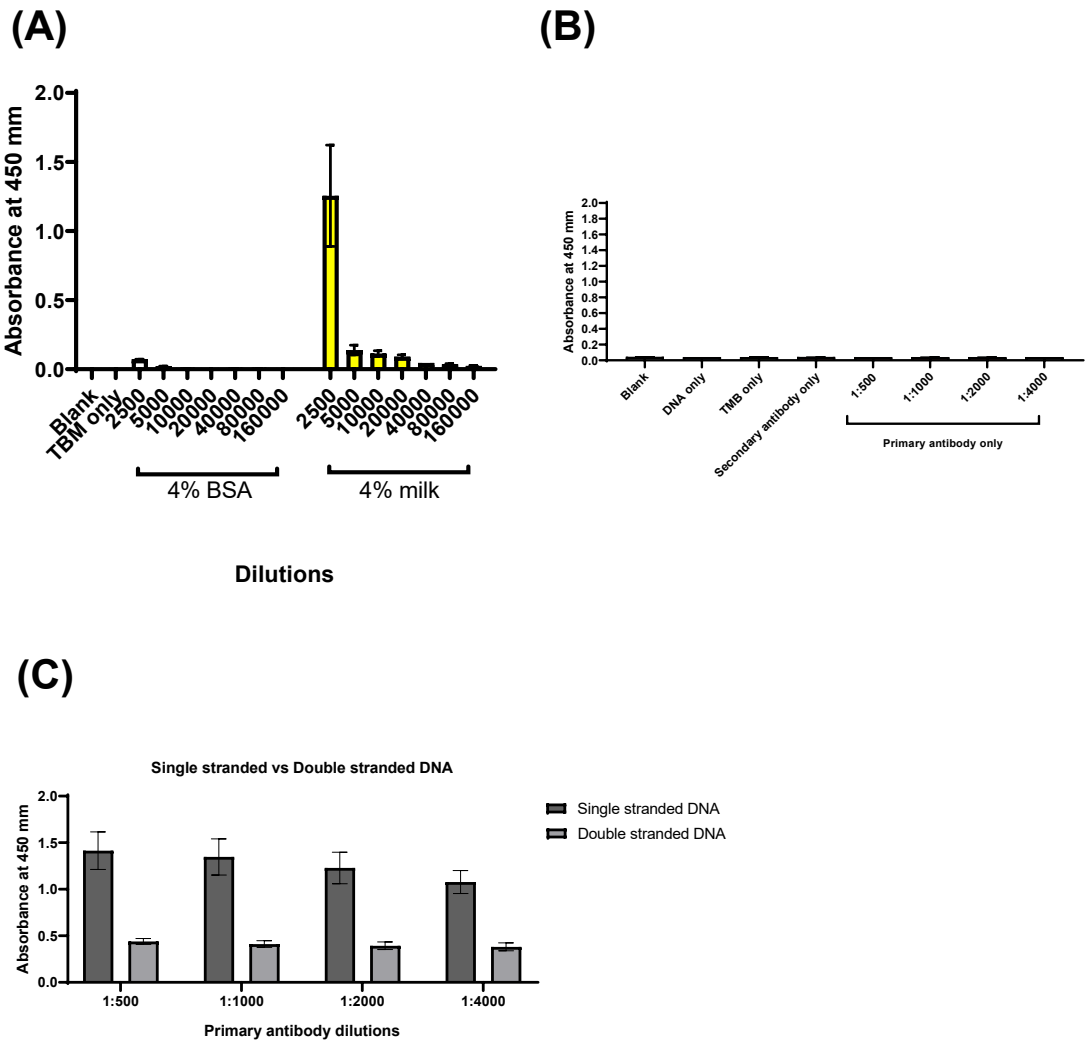

Figure 3. 10 Optimization of ELISA (A, B) blocking buffer solution, secondary antibody concentration, and (C) thymine dimer primary antibody concentration. (A) 4 % BSA had lower absorbance than (B) 4 % milk. UVC irradiated (C) single-stranded calf thymus DNA was higher absorbance (450 mm) than double-stranded DNA. Calf thymus DNA was irradiated with 0.12 J/cm^2 UVC before being made single-stranded. Different dilutions of primary antibody (anti-CPD) were used with secondary antibody (rat anti-mouse IgG1, HRP conjugated). Data represent mean ± SEM of duplicate determinations from n=3 individual experiments

CHAPTER 4

Investigation of the formation and repair of UV-induced, bulky DNA adducts in the nuclear and mitochondrial genomes.

This chapter has been published:

Alaa S. Alhegaili, Yunhee Ji, Nicolas Sylvius, Matthew J. Blades, Mahsa Karbaschi, Helen G. Tempest, George D. D. Jones, and Marcus S. Cooke

Genome-Wide Adductomics Analysis Reveals Heterogeneity in the Induction and Loss of Cyclobutane Thymine Dimers across Both the Nuclear and Mitochondrial Genomes

International Journal of Molecular Sciences. 2019

Volume 20 (20), 5112 pages

https://doi.org/10.3390/ijms20205112

Overview of Chapter 4

DNA damage and repair are considered to be key factors in the development of many diseases. There are many techniques used to measure DNA damage in the global genome, such as the alkaline comet assay, HPLC-MS/MS, or PCR. However, these methods cannot measure gene/sequence-specific levels of DNA damage in the nucleus, and mitochondria, which is important as the damage is not homogeneously distributed across the genome. In this chapter, Damaged DNA Immunoprecipitation, and next-generation sequencing (DDIP-seq) was applied to study the sequence-specific induction of nDNA and mtDNA damage (T<>T), induced by solar simulated radiation. Data on sequence-specific damage to nDNA is a relatively recent addition to the literature and is not widely reported, and for mtDNA, there is only one other report [72]. The results from this chapter showed that levels of mtDNA damage were much higher than nDNA, and there was a decrease of T<>T levels in both nDNA and mtDNA. Although there was no existing data of mechanism of repair of T<>T levels in mtDNA, the results from both DDIP-seq and PCR showed that T<>T levels were decreased in mtDNA after 24 h. However, further studies are required to explore the repair pathway(s) for T<>T in mtDNA.

Aim

To investigate the formation and repair of UV-induced DNA damage in nDNA versus mtDNA of human keratinocytes.

Methods

HaCaTs were maintained as described in section 2.1.1.1, chapter 2. Cells were irradiated with 0.1 J/cm^2 solar-simulated irradiation, or 0.12 J/cm^2 UVC, or 0.5 J/cm^2, or UVB, or

and treated with 50 μM H_2O_2, as described in section 2.1.2, chapter 2. For DDIP-seq, ELISA, and quantification of mtDNA damage and mtDNA copy number, the methods described in 2.4, chapter 2, were followed.

Results

4.1 Evaluation of Anti T<>T antibody specificity in thymine dimer using ELISA

Based on the manufacturer's commercial protocols for the DDIP-seq and anti-T<>T Mab, the ratio of the concentration of DNA and antibody (1.0:1.0 μg/mL) was used for DDIP-seq. For the additional characterization of antibody specificity, ELISA was used to evaluate the antibody specificity of the T<>T. The results from both double-stranded DNA and single-stranded DNA irradiated 0.12 J/cm^2 UVC only showed absorbance at 450 nm ($P<0.0001$). In addition, 1.0 μg/mL concentrations of antibody showed the highest absorbance at 450 nm (double-stranded: 0.439, and single-stranded:1.414) (Figure 4.1).

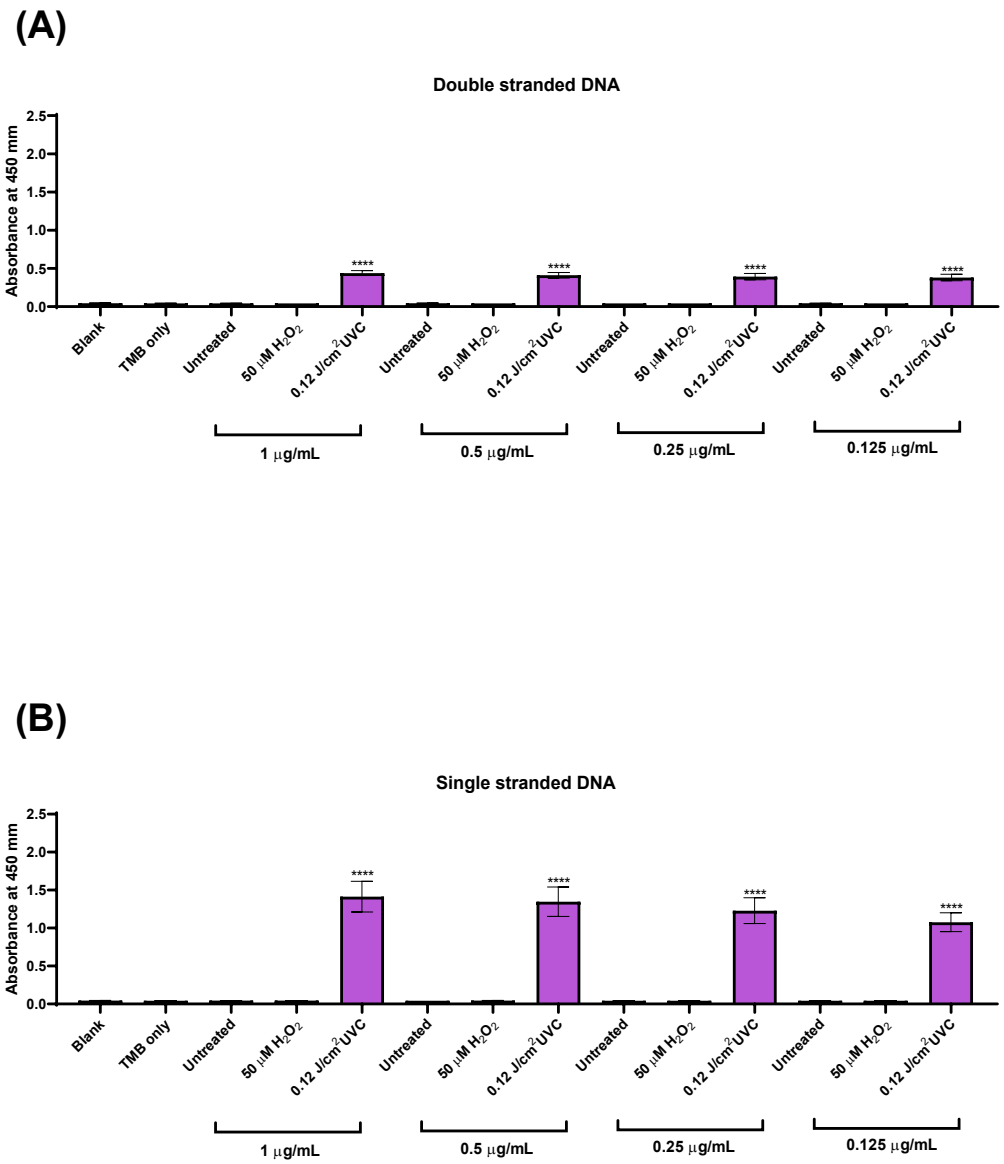

Figure 4. 1 Specificity of the anti- T<>T MAb determined by ELISA. (A) Double-stranded DNA (B) single-stranded DNA (boiled and rapidly cooled prior to performing ELISA) exposed to 50 μM H_2O_2, or 0.12 J/cm^2 UVC were used. Data represent the mean ±SEM of three independent experiments. **** represents P<0.001 One-way ANOVA was used for the statistical analysis.

4.2 Nuclear and mitochondrial genome-wide mapping of T<>T induction and repair.

To study the specific damaged gene regions and their repair, 13,680 genes in SSR irradiated HaCaTs were identified. Figure 4.2 illustrates the representative mapping data of T<>T in the whole nuclear genome in (A) chromosome 11 (7134 kb) and (B) chromosome 7 (7605 kb). The blue bars represent distribution, and levels of T<>T immediate irradiation (0 h) and red bars represent after 24 h of irradiation. The levels of some of T<>T were decreased after 24 h irradiation. However, some of the damage still remained remarkably high or increased after 24 h.

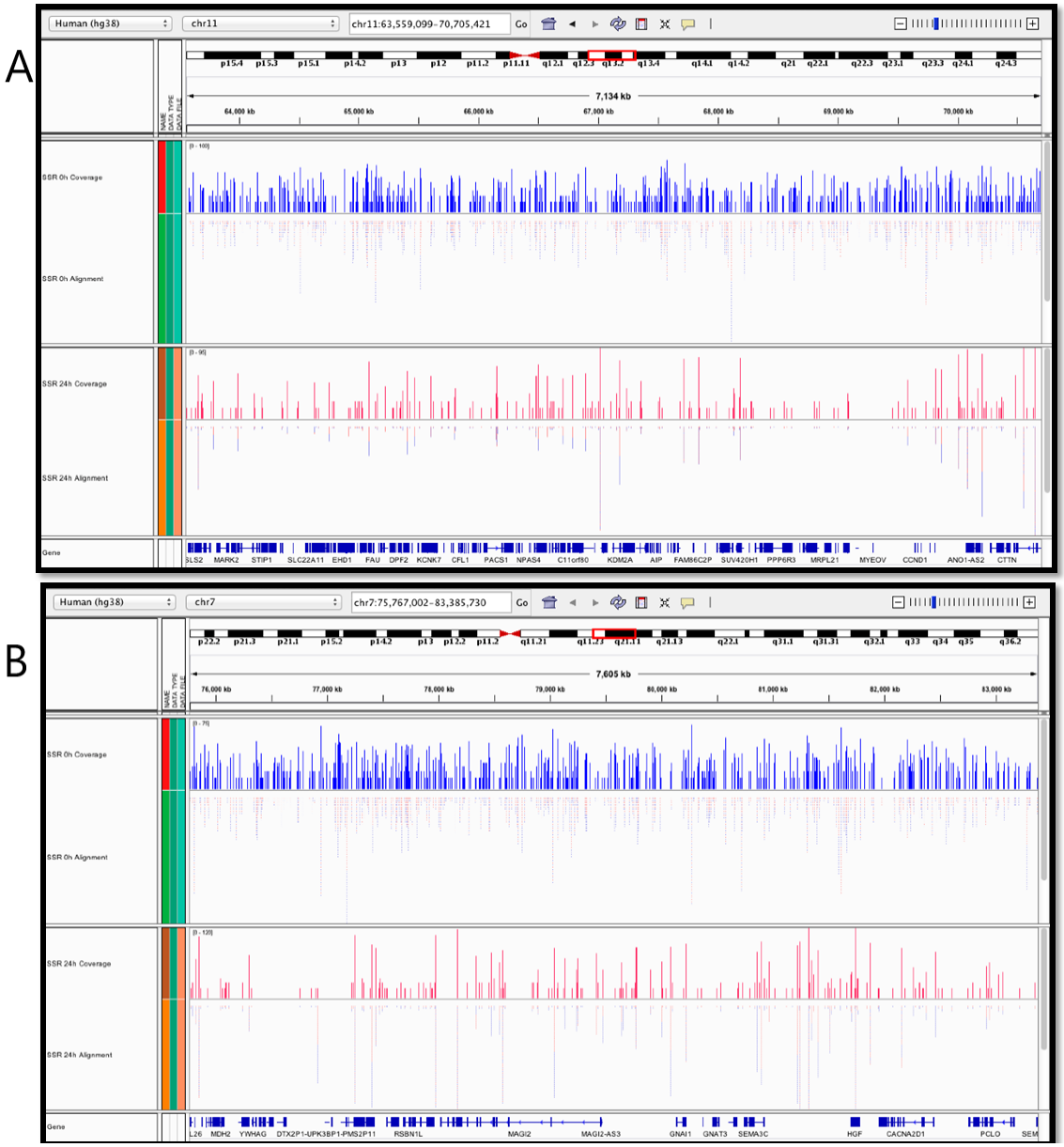

Figure 4. 2 Screenshot of a representative Integrated Genomic Viewer image after alignment of SSR-irradiated samples at 0 h and after 24 h of exposure. Each peak shows the levels of damage in HaCaTs irradiated with SSR and collected at 0 (blue) or 24 h (red) after irradiation. The data was mapped using human genome reference GRCh38 at (A) chromosome 11, q13.2 (7134 kb) (B) chromosome 7, q21.11 (7605 kb).

4.3 Levels of T<>T in both chromosomes and genes decreased after 24 h.

The distribution of damage between entire chromosomes was analyzed. Levels of T<>T per chromosome after irradiation and 24 h after irradiation were illustrated in Figure 4.3.A. The levels of T<>T per chromosome correlated with chromosome length and decreased at least 50 % after 24 h irradiation when compared with immediate radiation. In addition, the numbers of T<>T containing genes per chromosome showed a similar distribution of damage in each chromosome and were decreased in 24 h post-exposure than immediately SSR exposure (Figure 4.3.B). The most reduced number of genes containing T<>T was in chromosome 12, which decreased around 50 %.

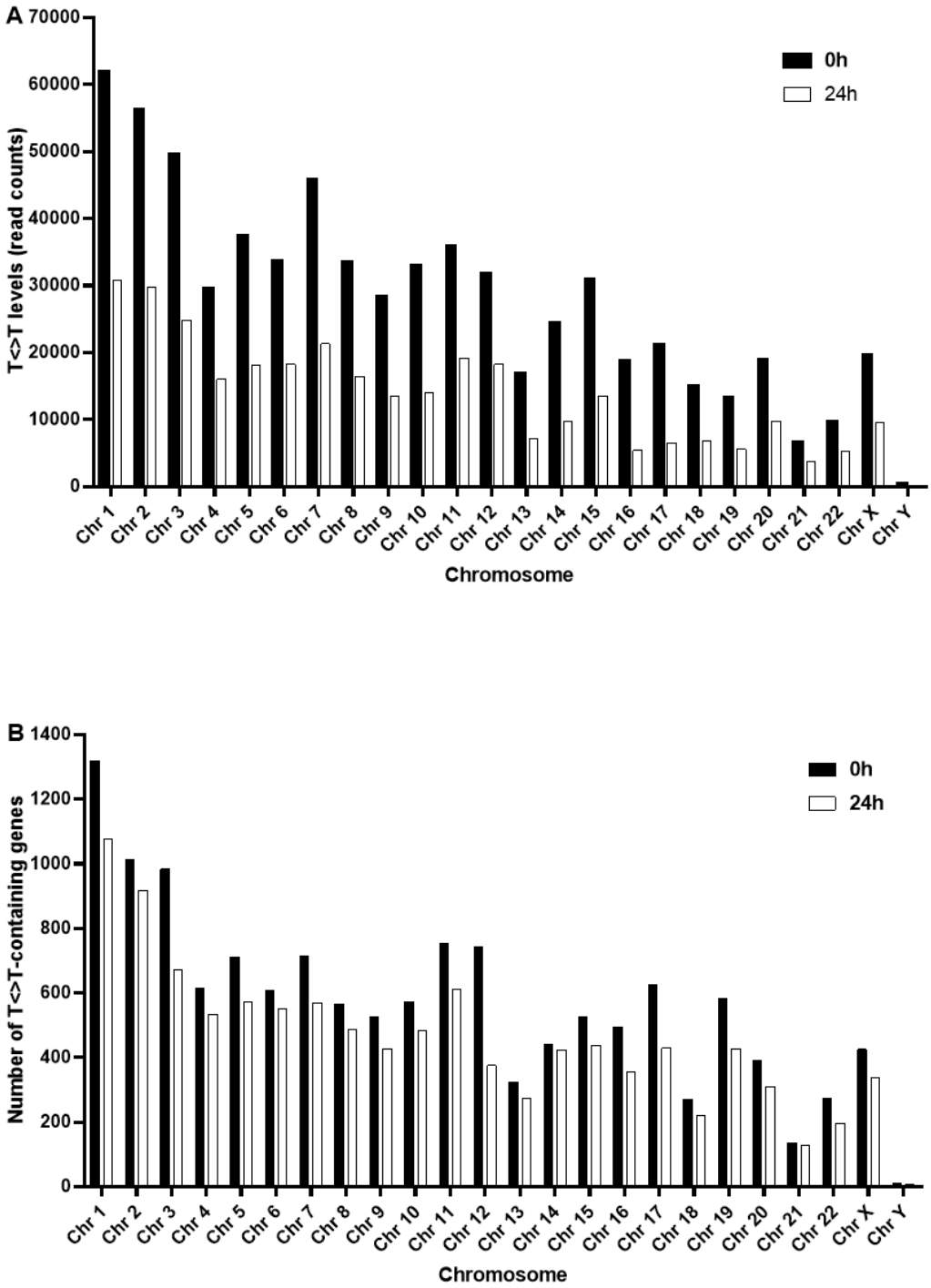

Figure 4. 3 Distribution of T<>T levels between chromosomes immediately after SSR irradiation (Black) and 24 h post-irradiation (White) in HaCaTs. The illustration shows (A) The levels of total T<>T per chromosome and (B) The numbers of damaged genes per chromosome, mapped to human genome assembly GRch35.

4.4 Levels of T<>T in both nuclear and mitochondrial genomic regions decreased 24 h after SSR irradiation.

Some of the genes in nuclear DNA showed the differential sensitivity of the formation after SSR irradiation shown in Figure 4.4.A. The highest DNA damage was shown in *WWOX* and *AGBL4,* which was more than 200 of DNA damage levels. After 24 h of post-irradiation, although *WWOX* had 96 % of DNA damage remaining and 66 % of DNA damage in *AGBL4*, other genes, such as *NCK2*, *ZRANB1*, *PUM2* and *SEL1* showed a decrease of T<>T damage to 0 % (Figure 4.4.B). The DNA damage in mitochondrial genomic regions was analyzed. The damage in mitochondrial genomic regions was higher than nuclear genomic regions (Figure 4.4.C). Removing the T<>T in nuclear DNA was shown to be more effective than mitochondrial regions, but levels of T<>T was decreased in mitochondrial regions especially, *ND1* and *ND2* genes. *CYB* and *ND5* had the highest DNA damage levels immediately following irradiation, but these declined to 53 and 52 % after 24 h post-irradiation (Figure 4.4.D).

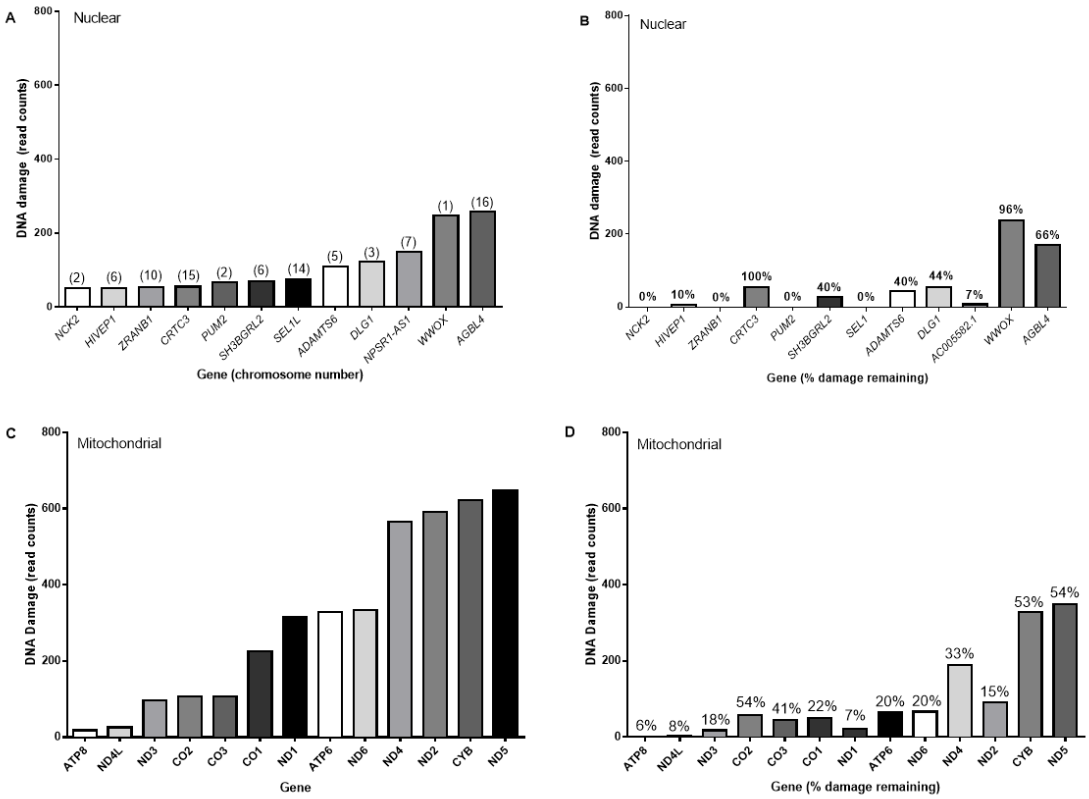

Figure 4. 4 Levels of T<>T regions immediately after SSR irradiation in (A) nuclear and (C) mitochondrial regions and percentage DNA remaining after 24 h post-irradiation in (B) nuclear and (D) mitochondrial regions. The data illustrate the differential DNA damage response of nuclear DNA and mitochondrial DNA.

4.5 qPCR confirmed that T<>T in the mitochondrial genome were decreased 24 h post-exposure to SSR.

Short-range qPCR was used for an alternative approach to confirm the time-independent loss of UV induced T<>T regions in the mitochondrial genome. The regions from *Cytb* to *ND6* genes showed that the damage caused by UVC, which is the most effective method to induce T<>T regions were decreased after 6 h post-irradiation and after 24 h and 48 h showed no significant differences when compared with the DNA not exposed to UVC (Figure 4.5.A). The mitochondrial copy number analysis was performed to investigate whether a change in mitochondria copy number could 'dilute' mitochondrial DNA damage, and therefore appear to give a decrease in damage levels. There was no significant difference in mitochondrial copy number between immediate UVC irradiation and any other time points of post-irradiation (Figure 4.5.B).

UVB irradiation was used as a relevant, environmental source of T<>T in human skin, and is the predominant wavelength in SSR effective at inducing T<>T. The results with UVB were similar to those with SSR and showed that immediate irradiation with UVB has significantly different showed ($P<0.001$). However, the damage at 24 h and 48 h of post-irradiation, there were no significant differences observed when compared with unirradiated samples. In addition, mitochondrial DNA contents were analyzed, and they were not significantly different as shown in the results (Figure 4.6.B)

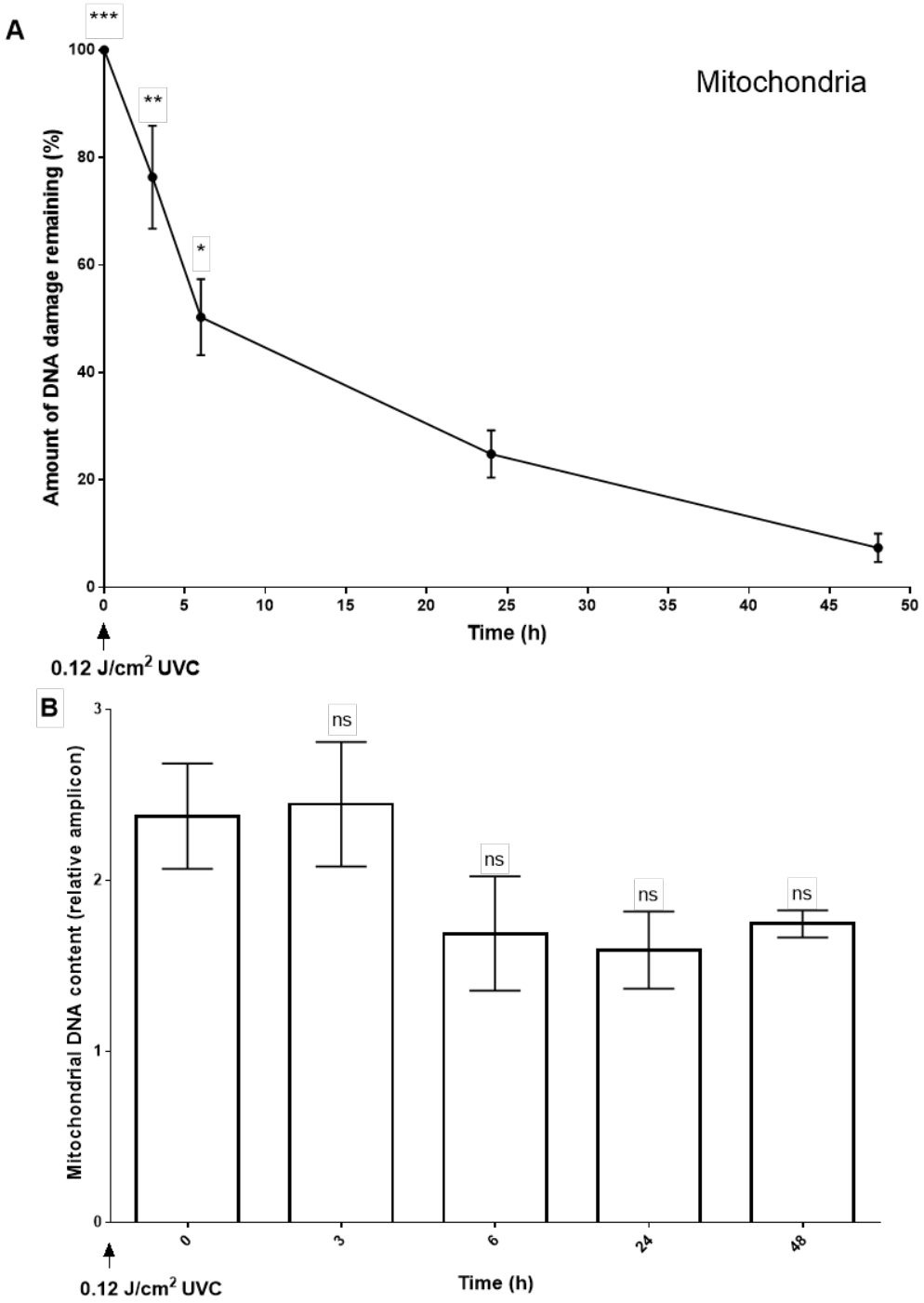

Figure 4. 5 (A) Loss of T<>T induced by UVC in mitochondrial genome determined by short-range qPCR and (B) mitochondrial DNA contents analysis were performed by real-time qPCR. The data represents the mean ±SEM of the n=3 independent experiment. *** $p<0.001$, $p<0.01$, $p<0.05$ and not significant (ns) related to (A) unirradiated samples (B) immediate irradiation (0 h).

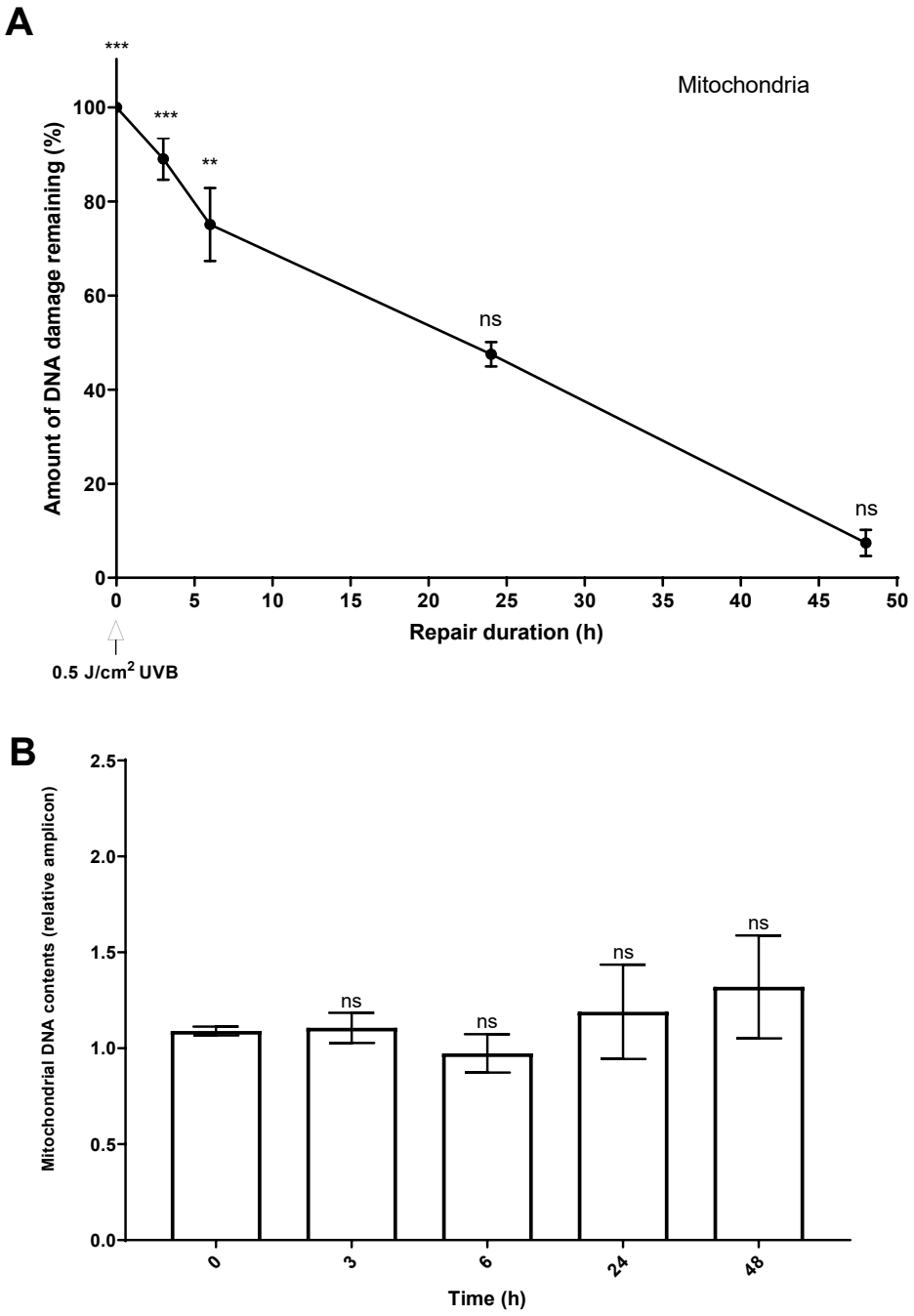

Figure 4. 6 (A) Loss of UVB induced T<>T and (B) mitochondrial genome contents in HaCaTs determined by qPCR. (A) Short-range PCR was performed to calculate lesion frequency to detect DNA damage. (B) relative amplification of mitochondrial DNA contents was calculated. Data represent ±SEM from n=3 individual experiments. A one-way ANOVA Tukey post hoc test was performed by the log-transformed value of mtDNA contents value.

Discussion

Many studies have used various methods to study DNA damage and repair at the level of the nuclear genome [66-68]. In this study, for the first time, we have mapped the formation and repair of T<>T across the entire nuclear and mitochondrial genomes. We have shown that there were specific regions susceptible to damage formation and confirmed a differential response of damage repair. It is not yet clear the fundamental reason for the differential response to the DNA damage and repair. However, this variation of response to DNA damage might be associated with inter-related elements such as nuclear organization, nucleotide sequences, DNA-histone interactions, and epigenetic factors [67, 73-80].

Many studies have explored mitochondrial DNA damage, and many methods have been used to analyze the mitochondrial DNA damage and response. However, with one exception, there have been no studies mapping damage across the whole mitochondrial genome, and certainly not mapping T<>T. We are the first study to map the induction and loss of T<>T across the mitochondrial genome. Like the nuclear genome, the mitochondrial genome also showed non-random distribution and differing levels of damage in each gene. Some of the damage was significantly higher in some genes, which implies that some loci were targeted preferentially. In addition, the levels of T<>T were higher in mitochondrial DNA compared to nuclear DNA. The results from both DDIP-seq and qPCR data showed that T<>T damage in both mitochondrial and nuclear DNA decreased with time. These results are surprising since mitochondrial have no NER pathway to remove T<>T in mammalian cells. The possibility is mitochondria degrade damaged DNA or rescue the undamaged DNA using a fusion pathway [81-83]. However, we have measured the

mtDNA content of UV irradiated cells with a time course, and there were no changes in mtDNA contents in all time points. Further studies are needed to determine the mechanism of the repair or remove of T<>T in mitochondrial.

Conclusion

This study investigated the DNA damage (T<>T) and repair in both nuclear and mitochondrial genome for the first time. These findings have not shown the specific mechanisms of repair, but we clearly demonstrated that there was the removal of T<>T in the mitochondrial genome.

The mapping approach using DDIP-seq provides a valuable understanding of the formation and repair of damage, and it might help investigate disease development and/or progression.

CHAPTER 5

Investigation of the effect of chronic bacterial infection on nuclear DNA damage and repair

This chapter has been published:

Yunhee Ji, Mahsa Karbaschi, Marcus S Cooke

Mycoplasma infection of cultured cells induces oxidative stress and attenuates cellular base excision repair activity

Mutation Research/Genetic Toxicology and Environmental Mutagenesis (2019)

Volume 845, 403054

https://doi.org/10.1016/j.mrgentox.2019.05.010.

Overview of Chapter 5

Mycoplasma contamination is a major concern for *in vitro* cell culture models as it is resistant to most antibiotics, which makes the prevention and treatment of infection challenging. Furthermore, numerous studies show that Mycoplasma infection alters a variety of cellular processes in a wide range of cell lines. However, there is a lack of information pertaining to the effects of Mycoplasma infection on genomic stability. In this study, a dopaminergic neuronal cell line (BE-M17), a popular *in vitro* model for studying Parkinson's disease, was used to evaluate the effect of Mycoplasma infection on genomic instability and base excision repair (BER) activity, using single-cell gel electrophoresis (the comet assay). The results showed that Mycoplasma infection-induced oxidative stress in the absence of an inflammatory response, with markedly increased levels of DNA damage, compared to uninfected cells. The source of the oxidative stress may have been increased ROS generation, or attenuation of cellular antioxidant capacity (or a combination of both). Uninfected cells initially repaired SB/ALS more rapidly than infected cells, although SB/ALS was fully repaired in both uninfected and infected cells 2 h after H_2O_2 challenge. However, while uninfected cells showed complete repair of oxidized purines within 24 h, for the infected cells, these were not fully repaired even after 30 h.

In conclusion, this study showed that not only does Mycoplasma infection induce oxidative stress and DNA damage, but it also decreases the efficiency of the main pathway responsible for the repair of oxidatively damaged DNA, i.e., BER. In this *in vitro* model, there is no mechanism for infection-induced inflammation, which could be a source of increased ROS production. Therefore, further studies are needed to evaluate how

Mycoplasma infection causes oxidatively damaged DNA and how it modulates cellular DNA repair.

Aim

To investigate the effect of chronic bacterial infection as an environmentally relevant source of genotoxicity, on DNA damage and repair in an *in vitro* model.

Methods

Mycoplasma infected and uninfected BE-M17 were grown according to the conditions described in chapter 2, section 2.5.1, and treated with 50 μM H_2O_2 prior to performing alkaline and alkaline hOGG1-modified comet assay to induce DNA damage in mycoplasma infected and uninfected cells. Mycoplasma infection was confirmed using the PCR method in a cell culture facility at Florida International University. All the procedure of methods was detailed in chapter 2, section 2.5.

Results

5.1 Confirmation of Mycoplasma infection

PCR analysis confirmed the presence of Mycoplasma in the culture of BE-M17 cells (Figure. 5.1). Confirmation was by the presence of a band at 500 bp (lanes 4 and 5), which was also seen in a positive control (DNA from an infected HepG1 cell line; lane 6). Comparison of the band intensities for BE-M17 and HepG1- DNA revealed high levels of infection in the former.

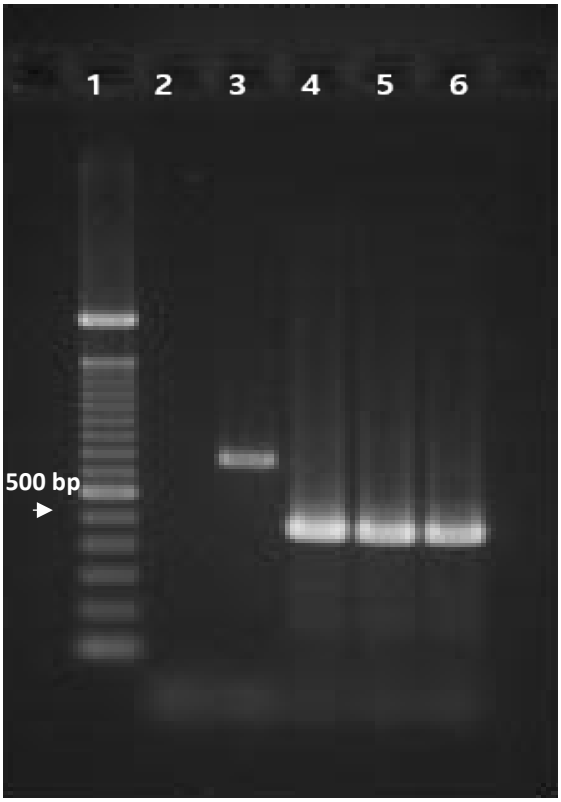

1. 100 bp DNA ladder
2. Control (no DNA)
3. Negative control
(DNA from uninfected cells)
4. BE-M17 infected
(DNA prep #1)
5. BE-M17 infected
(DNA prep #2)
6. Positive control
(DNA from Mycoplasma
infected HepG1 cells)

Figure 5. 1 Confirmation of Mycoplasma infection. Cells were cultured without antibiotics for at least two weeks prior to DNA extraction and PCR. DNA extraction and PCR were performed by the core cell culture facility at Florida International University.

5.2 Mycoplasma infection may be visualized during the comet assay

The gel background surrounding the comets, in the absence of Mycoplasma infection, was dark and clear of any debris (Figure. 5.2A and C). In contrast, for the Mycoplasma infected cells, the gel background showed a large amount of small, PI-stained (i.e., DNA-containing) particles, which we took to be associated with the Mycoplasma infection (Figure 5.2B and D). Supportive of this, the examination of the background of an unrelated, uninfected cell type (HaCaT keratinocyte), that had been run in parallel, showed no background staining (Figure. 5.2E). The nucleoids of both infected and uninfected BE-M17 cells appeared to have halo-like fluorescent rings around them, which seemed to be cell-type specific, and independent of infection, as these were absent from the HaCaTs.

.

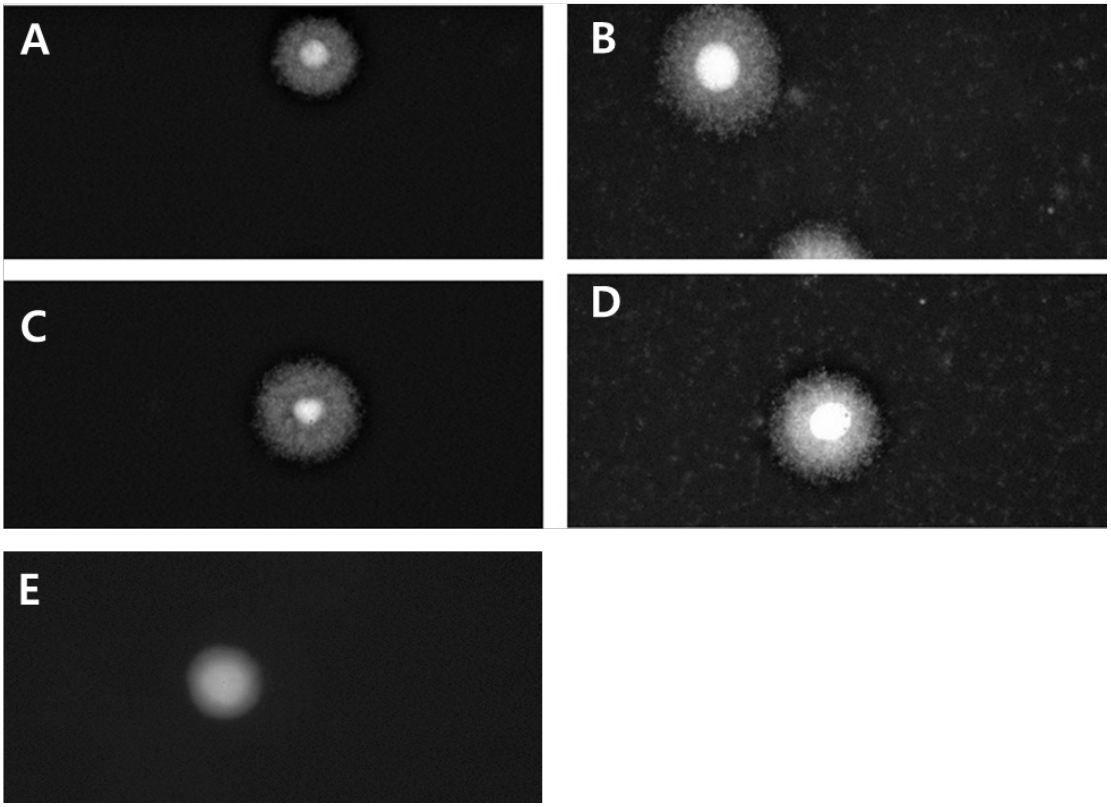

Figure 5. 2 Comparison of comet images between (A, C) Mycoplasma uninfected, (B, D) Mycoplasma infected BE-M17 cells, and (E) uninfected HaCaT keratinocytes. Cells were embedded in 0.6 % LMP agarose on 1% agarose pre-coated slides, and comet assay performed. After propidium iodide staining, fluorescence microscopy at 40X magnification was performed to visualize the cells.

5.3 Mycoplasma infection induces nuclear DNA damage

Mycoplasma infection induced a modest, 1.5-fold increase in background levels of SB/ALS (Figure. 5.3A and 3B). In contrast, levels of oxidized purines in BE-M17 increased 8.4-fold in the infected cells (Figure. 5.3A and 3B). After challenging the cells with 50 μM H_2O_2, levels of both SB/ALS and oxidized purines increased in both infected and uninfected cells. However, the increase in damage was approximately 1.3 times greater in the infected cells, compared to the uninfected cells (Figure. 5.3C) and applied approximately equally to both SB/ALS and oxidized purines.

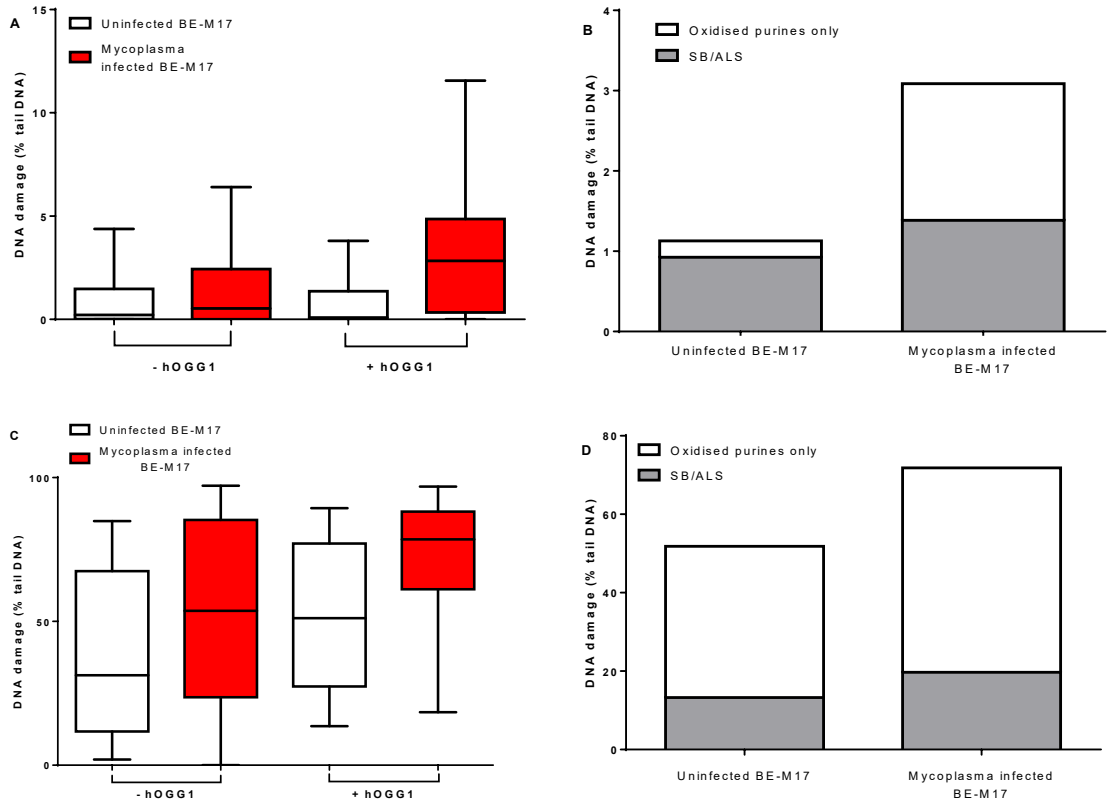

Figure 5. 3 Mycoplasma infection promotes the formation of DNA damage. hOGG1-modified comet assay was performed on Mycoplasma infected (red bars) and uninfected (white bars) BE-M17 cells: (A) box and whisker plots represent the median, maximum, and minimum of baseline comet % TD, with and without hOGG1-pretreatment prior to comet assay; (B) mean, baseline levels of SB/ALS and oxidized purines; (C) box and whisker plots represent the median, maxima, and minima of H_2O_2-induced DNA damage, with and without hOGG1-pretreatment prior to comet assay; and (D) mean levels of H_2O_2-induced SB/ALS and oxidized purines. Data are derived from n=2 individual experiments (100 determinations from each experiment).

5.4 Mycoplasma infection attenuates the repair of oxidized purines, but not SB/ALS

Although uninfected cells were marginally faster in repairing SB/ALS than infected cells over the first 1.5 h (Figure 5.4A, inset), levels of SB/ALS had returned to baseline levels in both uninfected and infected cells within 2 h of the induction of DNA damage with 50 μM H_2O_2 (Figure. 5.4A). This was despite infected cells having levels of SB/ALS 1.5 times greater than those of uninfected cells (Figure. 5.3D). In the uninfected cells, levels of oxidized purines increased marginally during the first hour following H_2O_2 exposure, before rapidly decreasing and reaching baseline levels within 24 h (Figure. 5.4B). In contrast, levels of oxidized purines increased 2.3-fold in the infected cells, in the 2 h following H_2O_2 exposure. Levels then slowly decreased, although levels remained high even at 30 h post-treatment with H_2O_2 (Figure. 5.4B).

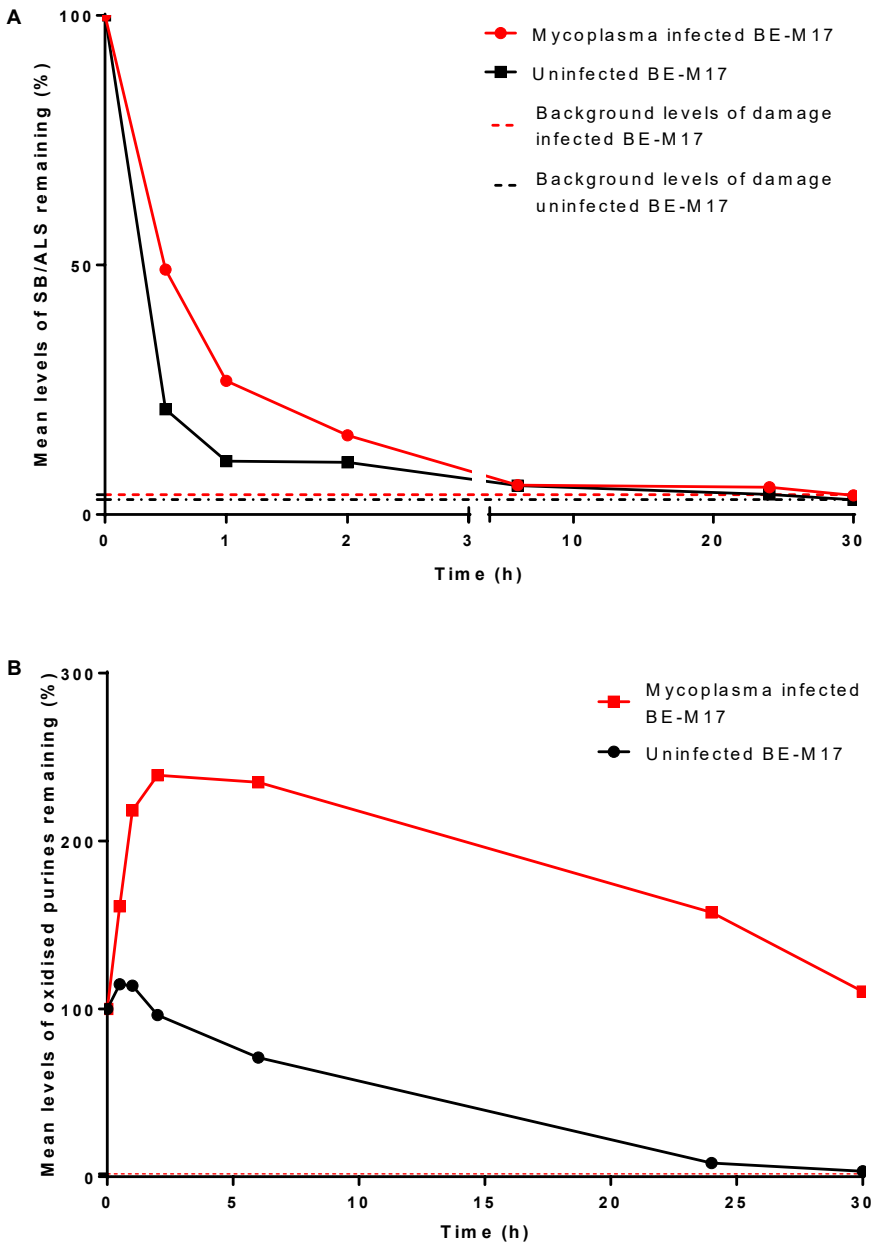

Figure 5. 4 Mycoplasma infection attenuates the repair of (A) SB/ALS and (B) oxidized purines. After treatment with 50 µM H_2O_2 for 30 min on ice, cells were allowed to repair for different durations (0, 30 min, 1 h, 2 h, 6 h, 24 h or 30 h). The hOGG1-modified comet assay was used to measure (A) SB/ALS, and (B) oxidized purines in infected (red) and uninfected (white) BE-M17 cells. Data represent mean values and calculated to % damage remaining from n=2 individual experiments (100 determinations from each experiment).

Discussion

Mycoplasma infection of cultured cells can be considered a stealthy condition. In the absence of testing for infection or a concerted effort to screen for subtle alterations in metabolism, experiments may be performed using cells that may be exhibiting an abnormal phenotype. The initial aim of this work was to characterize the DNA damage response in BE-M17 cells. However, the presence of a potential Mycoplasma infection was indicated during the scoring of comets due to a high background PI staining of the gels, even though the BE-M17 cells appeared to be grown normally. Based upon evidence that mitochondria cannot be visualized in the comet assay[84], we were skeptical that bacterial infection could account for the high background staining visible at the scoring step, particularly following lysis and electrophoresis. In the absence of any other explanation, we screened the BE-M17 cells to rule out Mycoplasma, but the results were positive. Uninfected cells showed no background, whereas Mycoplasma infected cells had a high background PI staining. We concluded that a high background at scoring could potentially warn of Mycoplasma infection. This is surprising, given that the comet assay lysis buffer consists of high salt and detergent, which removes all organelles and structures, including mitochondria, membrane, and proteins in the cells [85, 86], and that the Mycoplasma genome is markedly smaller than that of eukaryotes. Indeed, it is also one of the smallest genomes of the prokaryotes [87]. We speculate that visualization is only possible at high levels of Mycoplasma infection. Hence, the cause of any background staining in the comet assay should be investigated. As such, the comet assay could potentially serve as a viable method of Mycoplasma detection because this method is less expensive than other methods such as ELISA or real-time PCR, and where routine screening is not performed [23, 88].

Further studies are needed to evaluate what levels of Mycoplasma contamination are required in order to be detectable during scoring. Nonetheless, we strongly advocate routine Mycoplasma screening, for example by PCR.

The main endpoints of the alkaline comet assay are SB/ALS. They may be produced under conditions of oxidative stress, as a result of ROS generated during metabolism, or other endogenous processes, or exposure to environmental factors such as solar ultraviolet radiation [89, 90]. Our present data indicate that Mycoplasma infection induces oxidative stress and the formation of oxidatively modified DNA, perhaps via the depletion of cellular antioxidant defenses, rendering the BE-M17 cells more sensitive to ROS-induced DNA damage [22, 91]. Consistent with this, *in vitro* and *in vivo* studies show that Mycoplasma infection of lung cells results in oxidative stress, and DNA damage, as relevant models of lung infection [91, 92]. More specifically, our results demonstrated that Mycoplasma infection appears to preferentially increase levels of oxidized purines over SB/ALS. Our data, investigating the repair of SB/ALS and oxidized purines, may shed some light on this differential effect. Indeed, while BER of SB/ALS was unaffected, BER of oxidized purines was severely attenuated in the infected cells, and hence may explain the results seen previously [91, 92]. We also note a large, sustained increase in oxidized purines, that persists for 2 h after the H_2O_2 challenge. It is possible that Mycoplasma depletion of intracellular antioxidants increases the half-life of H_2O_2, and other ROS, some of which may preferentially oxidized purines, over SB formation [93]. We speculate that this, coupled with the oxidation of key repair proteins involved in the BER of oxidized purines, e.g., hOGG1, and for which there is ample precedent [94-96], could lead to the decrease in BER, and the initial, net increase in oxidized purines we noted.

Conclusion

High levels of Mycoplasma contamination results in background PI staining, which can be visualized during scoring in the comet assay. Additionally, we demonstrated that not only does Mycoplasma infection induce oxidative stress and DNA damage, but it also affects the main pathway responsible for the repair of oxidatively damaged DNA, and specifically the BER of oxidized purines. The limitation of the study was we are only able to perform the experiments twice for some experiments, so we were not able to perform any statistical analysis. In addition, we were only able to study in BE-M17, so further studies are needed to investigate these findings in other cell lines, and to investigate the mechanisms by which Mycoplasma infection causes DNA damage in the absence of a ROS-producing inflammatory response and how it interferes with a specific DNA repair pathway.

OVERALL CONCLUSION

The purpose of this study was to develop, optimize and apply the methods to assess DNA damage in the global genome and investigate the effect of representative environmental toxicants (UV and mycoplasma) on DNA damage and repair in relevant *in vitro* models.

This dissertation contains a number of novel discoveries

1. In chapter 3, we optimized the comet assay to reduce the running cost and duration of analysis, compared to conventional comet assay. Many other methods to assess DNA damage, such as PCR and ELISA, were also optimized to increase the efficiency of each assay.
2. In chapter 4, we reported mapping T<>T across the entire mitochondrial genome using DDIP-seq technology for the first time. Although some of the genes such as *CYB*, *CO2¸ND5* had T<>T remaining at levels more than 50 % at 24 h post-radiation, most of the mitochondrial genes demonstrated a decrease of T<>T level to less than 10 % at 24 h post-radiation. Furthermore, from the results of mtDNA contents analysis, we have shown that there was no significant change in mtDNA contents at 24 h post-irradiation. These results indicate that there might be some cellular mechanism to remove or decrease levels of T<>T. However, to date there have been no reports in the literature of NER, the repair mechanism for T<>T in nuclear DNA, operating in mitochondria. Further studies are required to prove how T<>T regions in mtDNA are removed.

3. In the last chapter, we investigated the effect of chronic bacterial infection (Mycoplasma) on the DNA damage response in BE-M17. We were able to visualize the mycoplasma infection on the comet assay slides. For the first time, we showed that not only does Mycoplasma infection induce SB/ALS, but also oxidized purines. An additional novel finding was that Mycoplasma infection attenuates the repair of oxidized purines (BER) in BE-M17, but seemingly not ALS/SB.

In this study, we investigated DNA damage induced by two different exogenous factors (UV and Mycoplasma infection) and repair using different techniques (DDIP-seq, PCR, and the comet assay). These findings are the first steps to investigate the mechanisms of the varying response of the DNA repair pathway and cellular response to DNA damage induced by different environmental exposures.

REFERENCES

1. Griffiths, A.J.F., *Modern genetic analysis : integrating genes and genomes*. 2002, New York: W.H. Freeman and Co.

2. Vella, F., *Understanding DNA: The molecule and how it works: By C R Calladine and H R Drew. pp 220. Academic Press, London and San Diego. 1992. £15.00 ISBN 0-12-155086-9.* Biochemical Education, 1994. **22**(2): p. 107-107.

3. Griffiths, A.J.F., Miller, J.H., Suzuki, D.T., Lewontin, R.C., Gelbart, W.M., *Introduction to genetic analysis*. 2015.

4. DePamphilis, M.L., Blow, J.J., Ghosh, S. Saha, T., Noguchi, K., Vassilev, A., *Regulating the licensing of DNA replication origins in metazoa.* Curr Opin Cell Biol, 2006. **18**(3): p. 231-9.

5. Chan, D.C., *Mitochondria: dynamic organelles in disease, aging, and development.* Cell, 2006. **125**(7): p. 1241-52.

6. Young, M.J. and W.C. Copeland, *Human mitochondrial DNA replication machinery and disease.* Curr Opin Genet Dev, 2016. **38**: p. 52-62.

7. Alexeyev, M.,Shokolenko, I., Wilson, G., LeDoux, S., *The maintenance of mitochondrial DNA integrity--critical analysis and update.* Cold Spring Harb Perspect Biol, 2013. **5**(5): p. a012641.

8. Cooke, M.S., Evans, M.D., Dizdaroglu, M., Lunec J., *Oxidative DNA damage: mechanisms, mutation, and disease.* FASEB J, 2003. **17**(10): p. 1195-214.

9. Yang, Y., Bazhin, A.V., Werner, J., Karakhanova, S., *Reactive oxygen species in the immune system.* Int Rev Immunol, 2013. **32**(3): p. 249-70.

10. Evans, M.D. and M.S. Cooke, *Factors contributing to the outcome of oxidative damage to nucleic acids.* Bioessays, 2004. **26**(5): p. 533-42.

11. Roos, W.P. and B. Kaina, *DNA damage-induced cell death by apoptosis.* Trends Mol Med, 2006. **12**(9): p. 440-50.

12. Cadet, J., T. Douki, and J.L. Ravanat, *Oxidatively generated damage to cellular DNA by UVB and UVA radiation.* Photochem Photobiol, 2015. **91**(1): p. 140-55.

13. Cooke, M.S., Evans, M.D., Herbert, K.E., and Lunec, J., *Urinary 8-oxo-2'-deoxyguanosine--source, significance and supplements.* Free Radic Res, 2000. **32**(5): p. 381-97.

14. Lucas, R., *Global burden of disease from solar ultraviolet radiation.* Environmental burden of disease series, 2006. **13**.

15. Pfeifer, G.P. and A. Besaratinia, *Mutational spectra of human cancer.* Hum Genet, 2009. **125**(5-6): p. 493-506.

16. Premi, S., Wallisch, S., Mano, C.M., Weiner, A.B., Bacchiocchi, A., Wakamatsu, K., Bechara, E.J., Halaban, R., Douki, T., and Brash, D.E., *Photochemistry. Chemiexcitation of melanin derivatives induces DNA photoproducts long after UV exposure.* Science, 2015. **347**(6224): p. 842-7.

17. Cadet, J., Douki, T., Pouget, J.P., Ravanat, J.L., and Sauvaigo, S., *Effects of UV and visible radiations on cellular DNA.* Curr Probl Dermatol, 2001. **29**: p. 62-73.

18. Gale, J.M., K.A. Nissen, and M.J. Smerdon, *UV-induced formation of pyrimidine dimers in nucleosome core DNA is strongly modulated with a period of 10.3 bases.* Proceedings of the National Academy of Sciences, 1987. **84**(19): p. 6644-6648.

19. Zavala, A.G., Morris, R.T., Wyrick, J.J., and Smerdon, M.J., *High-resolution characterization of CPD hotspot formation in human fibroblasts.* Nucleic Acids Research, 2013. **42**(2): p. 893-905.

20. Schick, S., Fournier, D., Thakurela, S., Sahu, K.S., Garding, A., and Tiwari, V.K., *Dynamics of chromatin accessibility and epigenetic state in response to UV damage.* Journal of Cell Science, 2015. **128**(23): p. 4380-4394.

21. Nikfarjam, L. and P. Farzaneh, *Prevention and detection of Mycoplasma contamination in cell culture.* Cell J, 2012. **13**(4): p. 203-12.

22. Lincoln, C.K. and M.G. Gabridge, *Cell culture contamination: sources, consequences, prevention, and elimination.* Methods Cell Biol, 1998. **57**: p. 49-65.

23. Drexler, H.G. and C.C. Uphoff, *Mycoplasma contamination of cell cultures: Incidence, sources, effects, detection, elimination, prevention.* Cytotechnology, 2002. **39**(2): p. 75-90.

24. Sun, G., Xu, X., Wang, Y., Shen, X., Chen, Z., and Yang, J., *Mycoplasma pneumoniae Infection Induces Reactive Oxygen Species and DNA Damage in A549 Human Lung Carcinoma Cells.* Infection and Immunity, 2008. **76**(10): p. 4405-4413.

25. Wood, R.D., *Nucleotide excision repair in mammalian cells.* J Biol Chem, 1997. **272**(38): p. 23465-8.

26. Sancar, A., *DNA EXCISION REPAIR.* Annual Review of Biochemistry, 1996. **65**(1): p. 43-81.

27. Lodish, U.H., *Molecular Cell Biology*. 2016: W.H. Freeman.

28. Meng, E., Hanna, A., Samant, R.S., and Shevde L.A., *The Impact of Hedgehog Signaling Pathway on DNA Repair Mechanisms in Human Cancer.* Cancers (Basel), 2015. **7**(3): p. 1333-48.

29. Cooke, M.S., P.T. Henderson, and M.D. Evans, *Sources of extracellular, oxidatively-modified DNA lesions: implications for their measurement in urine.* J Clin Biochem Nutr, 2009. **45**(3): p. 255-70.

30. Shinmura, K., Yamaguchi, S., Saitoh, T., Takeuchi-Sasaki, M., Kim, S.R., Nohmi, T., and Yokota, J., *Adenine excisional repair function of MYH protein on the adenine:8-hydroxyguanine base pair in double-stranded DNA.* Nucleic Acids Res, 2000. **28**(24): p. 4912-8.

31. Hwang, B.J., G. Shi, and A.L. Lu, *Mammalian MutY homolog (MYH or MUTYH) protects cells from oxidative DNA damage.* DNA Repair (Amst), 2014. **13**: p. 10-21.

32. Martin, S.A., *Mitochondrial DNA repair. DNA Repair–On the Pathways to Fixing DNA Damage and Error.* 2011.

33. Kunkel, T.A. and D.A. Erie, *DNA mismatch repair.* Annu Rev Biochem, 2005. **74**: p. 681-710.

34. Prakash, A. and S. Doublie, *Base Excision Repair in the Mitochondria.* J Cell Biochem, 2015. **116**(8): p. 1490-9.

35. Sharma, M., Predeus, A.V., Kovacs, N., and Feig, M., *Differential mismatch recognition specificities of eukaryotic MutS homologs, MutSalpha and MutSbeta.* Biophys J, 2014. **106**(11): p. 2483-92.

36. Li, G.-M., *Mechanisms and functions of DNA mismatch repair.* Cell Research, 2008. **18**(1): p. 85-98.

37. Traver, S., Coulombe, P., Peiffer, I., Hutchins, J.R., Kitzmann, M., Latreille, D., and Mechali, M., *MCM9 Is Required for Mammalian DNA Mismatch Repair.* Mol Cell, 2015. **59**(5): p. 831-9.

38. Kunkel, T.A. and D.A. Erie, *Eukaryotic Mismatch Repair in Relation to DNA Replication.* Annu Rev Genet, 2015. **49**: p. 291-313.

39. Samsel, A. and S. Seneff, *Glyphosate's Suppression of Cytochrome P450 Enzymes and Amino Acid Biosynthesis by the Gut Microbiome: Pathways to Modern Diseases.* Entropy, 2013. **15**(4): p. 1416-1463.

40. Heu, C., Elie-Caille, C., Mougey, V., Launay S., and Nicod, L., *A step further toward glyphosate-induced epidermal cell death: involvement of mitochondrial and oxidative mechanisms.* Environ Toxicol Pharmacol, 2012. **34**(2): p. 144-153.

41. Simonian, N.A. and J.T. Coyle, *Oxidative stress in neurodegenerative diseases.* Annu Rev Pharmacol Toxicol, 1996. **36**: p. 83-106.

42. Vasko, M.R., C. Guo, and M.R. Kelley, *The multifunctional DNA repair/redox enzyme Ape1/Ref-1 promotes survival of neurons after oxidative stress.* DNA repair, 2005. **4**(3): p. 367-379.

43. Lovell, M.A., C. Xie, and W.R. Markesbery, *Decreased base excision repair and increased helicase activity in Alzheimer's disease brain.* Brain Res, 2000. **855**(1): p. 116-23.

44. Sheng, Z., Oka, S., Tsuchimoto, D., Abolhassani, N., Nomaru, H., Sakumi, K., Yamada, H., and Nakabeppu, Y., *8-Oxoguanine causes neurodegeneration during MUTYH-mediated DNA base excision repair.* The Journal of Clinical Investigation, 2012. **122**(12): p. 4344-4361.

45. Nakazawa, H., English, D., Randell, P.L., Nakazawa., K., Martel, N., Armstrong, B.K., and Yamasaki, H., *UV and skin cancer: specific p53 gene mutation in normal skin as a biologically relevant exposure measurement.* Proc Natl Acad Sci U S A, 1994. **91**(1): p. 360-4.

46. Daya-Grosjean, L., *Xeroderma pigmentosum and skin cancer.* Adv Exp Med Biol, 2008. **637**: p. 19-27.

47. Chang, N.-B., Feng, R., Gao, Z., and Gao, W., *Skin cancer incidence is highly associated with ultraviolet-B radiation history.* International Journal of Hygiene and Environmental Health, 2010. **213**(5): p. 359-368.

48. Armstrong, B.K. and A. Kricker, *How much melanoma is caused by sun exposure?* Melanoma Res, 1993. **3**(6): p. 395-401.

49. Zella, D., Curreli, S., Benedetti, F., Krishnan, S., Cocchi, F., Latinovic, O.S., Denaro, F., Romerio, F., Djavani, M., Charurat, M.E., Bryant, J.L., Tettelin, H., and Gallo, R.C., *Mycoplasma promotes malignant transformation in vivo, and its DnaK, a bacterial chaperone protein, has broad oncogenic properties.* Proceedings of the National Academy of Sciences, 2018. **115**(51): p. E12005-E12014.

50. Namiki, K., Goodison, Sl., Porvasnik, S., Allan, R.W., Iczkowski, K.A., Urbanek, C., Reyes, L., Sakamoto, N., and Rosser, C.J., *Persistent exposure to Mycoplasma induces malignant transformation of human prostate cells.* PLoS One, 2009. **4**(9): p. e6872.

51. Kennedy, C.H., Cueto, R., Belinsky, S.A., Lechner, J.F., and Pryor, W.A., *Overexpression of hMTH1 mRNA: a molecular marker of oxidative stress in lung cancer cells.* FEBS Lett, 1998. **429**(1): p. 17-20.

52. Collins, A.R., *The comet assay for DNA damage and repair.* Molecular Biotechnology, 2004. **26**(3): p. 249.

53. Ostling, O. and K.J. Johanson, *Microelectrophoretic study of radiation-induced DNA damages in individual mammalian cells.* Biochem Biophys Res Commun, 1984. **123**(1): p. 291-8.

54. Singh, N.P., McCoy, M.T., Tice, R.R., and Schneider, E.L., *A simple technique for quantitation of low levels of DNA damage in individual cells.* Exp Cell Res, 1988. **175**(1): p. 184-91.

55. Collins, A., Koppen, G., Valdiglesia, V., Dusinska, M., Kruszewski, M., Moller, P., Rojas, E., Dhawan, A., Benzie, I., Coskun, E., Moretti, M., Speit, G., Bonassi, S., and ComNet projet., *The comet assay as a tool for human biomonitoring studies: the ComNet project.* Mutat Res Rev Mutat Res, 2014. **759**: p. 27-39.

56. Olive, P.L., J.P. Banáth, and R.E. Durand, *Heterogeneity in radiation-induced DNA damage and repair in tumor and normal cells measured using the "comet" assay.* Radiat Res, 1990. **122**(1): p. 86-94.

57. Angelis, K.J., M. Dusinská, and A.R. Collins, *Single cell gel electrophoresis: detection of DNA damage at different levels of sensitivity.* Electrophoresis, 1999. **20**(10): p. 2133-8.

58. Karbaschi, M. and M.S. Cooke, *Novel method for the high-throughput processing of slides for the comet assay.* Scientific Reports, 2014. **4**(1): p. 7200.

59. Ge, J., Prasongtanakij, S., Wood, D.K., Weingeist, D.M., Fessler, J., Navasummrit, P., Ruchirawat, M., and Engelward, B.P., *CometChip: a high-throughput 96-well platform for measuring DNA damage in microarrayed human cells.* J Vis Exp, 2014(92): p. e50607.

60. Rooney, J.P., Ryde, I.T., Sanders, L.H., Howlett, E.H., Colton, M.D., Germ, K.E., Mayer, G.D., Greenamyre, J.T., and Meyer, J.N., *PCR based determination of mitochondrial DNA copy number in multiple species.* Methods Mol Biol, 2015. **1241**: p. 23-38.

61. Zhigalina, D.I., Skryabin, N.A., Vasilieva, O.Y., Lopatkina, M.E., Vasiliev, S.A., Sivokhha, V.M., Belyaeva, E.O., Savchenko, R.R., Nazarenko, L.p., and Levedev, I.N., *FISH Diagnostics of Chromosomal Translocation with the Technology of Synthesis of Locus-Specific DNA Probes Based on Long-Range PCR.* Russian Journal of Genetics, 2020. **56**(6): p. 739-746.

62. Hanna, R., Crowther, J. M., Bulsara, P. A., Wang, X., Moore, D. J., & Birch-Machin, M. A., *Optimised detection of mitochondrial DNA strand breaks.* Mitochondrion, 2019. **46**: p. 172-178.

63. Mansouri*, A., Gaou, I., de Kerguenec, C., Amsellem, S., Haouzi, D., Berson, A., ... and Fromenty, B.., *An alcoholic binge causes massive degradation of hepatic mitochondrial DNA in mice.* Gastroenterology, 1999. **117**(1): p. 181-190.

64. Zavala, A.G., Morris, R. T., Wyrick, J. J., & Smerdon, M. J., *High-resolution characterization of CPD hotspot formation in human fibroblasts.* Nucleic Acids Res, 2014. **42**(2): p. 893-905.

65. Amente, S., Di Palo, G., Scala, G., Castrignanò, T., Gorini, F., Cocozza, S., ... and Lania, L.., *Genome-wide mapping of 8-oxo-7,8-dihydro-2'-deoxyguanosine reveals accumulation of oxidatively-generated damage at DNA replication origins within transcribed long genes of mammalian cells.* Nucleic Acids Res, 2019. **47**(1): p. 221-236.

66. Crosetto, N., Mitra, A., Silva, M. J., Bienko, M., Dojer, N., Wang, Q., ... and Pasero, P. ., *Nucleotide-resolution DNA double-strand break mapping by next-generation sequencing.* Nature Methods, 2013. **10**(4): p. 361-365.

67. Yoshihara, M., Jiang, L., Akatsuka, S., Suyama, M., and Toyokuni, S., *Genome-wide Profiling of 8-Oxoguanine Reveals Its Association with Spatial Positioning in Nucleus.* DNA Research, 2014. **21**(6): p. 603-612.

68. James, R.P., Bennett, M., Waters, R., Skinner, N., and H Reed, S.., *Functional Genome-wide Analysis: a Technical Review, Its Developments and Its Relevance to Cancer Research.* Recent Patents on DNA & Gene Sequences (Discontinued), 2013. **7**(2): p. 157-166.

69. Hartmann, A., Agurell, E., Beevers, C., Brendler-Schwaab, S., Burlinson, B., Clay, P., ... and Tice, R. R., *Recommendations for conducting the in vivo alkaline Comet assay.* Mutagenesis, 2003. **18**(1): p. 45-51.

70. Karbaschi, M., *Investigation of ultraviolet radiation-induced DNA damage and repair in human skin cells*. 2012, University of Leicester. p. 266.

71. Cooke, M.S. and A. Robson, *Immunochemical detection of UV-induced DNA damage and repair.* Methods Mol Biol, 2006. **314**: p. 215-28.

72. Wauchope, O.R., Mitchener, M. M., Beavers, W. N., Galligan, J. J., Camarillo, J. M., Sanders, W. D., ... and deCaestecker, M.., *Oxidative stress increases M1dG, a major peroxidation-derived DNA adduct, in mitochondrial DNA.* Nucleic Acids Res, 2018. **46**(7): p. 3458-3467.

73. Ding, Y., A.M. Fleming, and C.J. Burrows, *Sequencing the Mouse Genome for the Oxidatively Modified Base 8-Oxo-7,8-dihydroguanine by OG-Seq.* J Am Chem Soc, 2017. **139**(7): p. 2569-2572.

74. Cooke, M.S.E., M.D, *Reactive Oxygen Species: From DNA Damage to Disease.* Sci. Med, 2010. **12**: p. 98-111.

75. Poetsch, A.R., S.J. Boulton, and N.M. Luscombe, *Genomic landscape of oxidative DNA damage and repair reveals regioselective protection from mutagenesis.* Genome Biology, 2018. **19**(1): p. 215.

76. Mitchell, D.L., J. Jen, and J.E. Cleaver, *Sequence specificity of cyclobutane pyrimidine dimers in DNA treated with solar (ultraviolet B) radiation.* Nucleic Acids Research, 1992. **20**(2): p. 225-229.

77. Carrell, D.T., *ANDROLOGY LAB CORNER*: The Clinical Implementation of Sperm Chromosome Aneuploidy Testing: Pitfalls and Promises.* Journal of Andrology, 2008. **29**(2): p. 124-133.

78. McLachlan, R.I. and M.K. O'Bryan, *State of the Art for Genetic Testing of Infertile Men.* The Journal of Clinical Endocrinology & Metabolism, 2010. **95**(3): p. 1013-1024.

79. Hotaling, J. and D.T. Carrell, *Clinical genetic testing for male factor infertility: current applications and future directions.* Andrology, 2014. **2**(3): p. 339-350.

80. Stahl, P.J., Masson, P., Mielnik, A., Marean, M. B., Schlegel, P. N., and Paduch, D. A., *A decade of experience emphasizes that testing for Y microdeletions is essential in American men with azoospermia and severe oligozoospermia.* Fertility and Sterility, 2010. **94**(5): p. 1753-1756.

81. Fakouri, N.B., Hou, Y., Demarest, T. G., Christiansen, L. S., Okur, M. N., Mohanty, J. G., ... and Bohr, V. A., *Toward understanding genomic instability, mitochondrial dysfunction and aging.* The FEBS Journal, 2019. **286**(6): p. 1058-1073.

82. Vasileiou, P.V.S., I. Mourouzis, and C. Pantos, *Principal Aspects Regarding the Maintenance of Mammalian Mitochondrial Genome Integrity.* Int J Mol Sci, 2017. **18**(8).

83. Meyer, J.N., T.C. Leuthner, and A.L. Luz, *Mitochondrial fusion, fission, and mitochondrial toxicity.* Toxicology, 2017. **391**: p. 42-53.

84. Shaposhnikov, S., et al., *Detection of Alu sequences and mtDNA in comets using padlock probes.* Mutagenesis, 2006. **21**(4): p. 243-247.

85. Langie, S.A., A. Azqueta, and A.R. Collins, *The comet assay: past, present, and future.* Front Genet, 2015. **6**: p. 266.

86. Azqueta, A. and M. Dusinska, *The use of the comet assay for the evaluation of the genotoxicity of nanomaterials.* Front Genet, 2015. **6**: p. 239.

87. Su, C.J. and J.B. Baseman, *Genome size of Mycoplasma genitalium.* Journal of Bacteriology, 1990. **172**(8): p. 4705-4707.

88. Woods, J.A., O'leary, K. A., McCarthy, R. P., and O'Brien, N. M., *Preservation of comet assay slides: comparison with fresh slides.* Mutat Res, 1999. **429**(2): p. 181-7.

89. Ramos-Espinosa, P., E. Rojas, and M. Valverde, *Differential DNA damage response to UV and hydrogen peroxide depending of differentiation stage in a neuroblastoma model.* Neurotoxicology, 2012. **33**(5): p. 1086-95.

90. Gabridge, M.G., *Metabolic consequences of Mycoplasma pneumoniae infection.* Isr J Med Sci, 1987. **23**(6): p. 574-9.

91. Sun, G., Xu, X., Wang, Y., Shen, X., Chen, Z., and Yang, J., *Mycoplasma pneumoniae infection induces reactive oxygen species and DNA damage in A549 human lung carcinoma cells.* Infect Immun, 2008. **76**(10): p. 4405-13.

92. Kariya, C., Chu, H. W., Huang, J., Leitner, H., Martin, R. J., and Day, B. J., *Mycoplasma pneumoniae infection and environmental tobacco smoke inhibit lung glutathione adaptive responses and increase oxidative stress.* Infect Immun, 2008. **76**(10): p. 4455-62.

93. Kennedy, L.J., Moore, K., Caulfield, J. L., Tannenbaum, S. R., and Dedon, P. C., *Quantitation of 8-oxoguanine and strand breaks produced by four oxidizing agents.* Chem Res Toxicol, 1997. **10**(4): p. 386-92.

94. Montaner, B., O'Donovan, P., Reelfs, O., Perrett, C. M., Zhang, X., Xu, Y. Z., ... and Karran, P., *Reactive oxygen-mediated damage to a human DNA replication and repair protein.* EMBO reports, 2007. **8**(11): p. 1074-1079.

95. Guven, M., Brem, R., Macpherson, P., Peacock, M., & Karran, P.., *Oxidative Damage to RPA Limits the Nucleotide Excision Repair Capacity of Human Cells.* J Invest Dermatol, 2015. **135**(11): p. 2834-2841.

96. Guven, M., Barnouin, K., Snijders, A. P., & Karran, P., *Photosensitized UVA-Induced Cross-Linking between Human DNA Repair and Replication Proteins and DNA Revealed by Proteomic Analysis.* J Proteome Res, 2016. **15**(12): p. 4612-4623.

VITA

YUNHEE JI

Born, Seoul, South Korea

2006-2010	B.S., Genetic Engineering Hankyung National University Anseong, South Korea
2010-2011	English language learning program Oregon State University Corvallis, Oregon
2012-2015	M.S., Biological Science University of Massachusetts- Lowell Lowell, Massachusetts
2015-2017	Graduate Assistant Florida International University Miami, Florida
2018-2020	Doctoral Candidate Florida International University Miami, Florida

PUBLICATIONS AND PRESENTATIONS

Karbaschi, M., Ji, Y., Abdulwahed, A. M. S., Alohaly, A., Bedoya, J. F., Burke, S. L., ... & Cooke, M. S. (2019). Evaluation of the Major Steps in the Conventional Protocol for the Alkaline Comet Assay. *International Journal of Molecular Sciences*, ***20***(23), 6072.

Alhegaili, A. S., Ji, Y., Sylvius, N., Blades, M. J., Karbaschi, M., Tempest, H. G, ... & Cooke, M. S. (2019). Genome-Wide Adductomics Analysis Reveals Heterogeneity in the Induction and Loss of Cyclobutane Thymine Dimers across Both the Nuclear and Mitochondrial Genomes. *International journal of molecular sciences*, ***20***(20), 5112.

Ji, Y., Karbaschi, M., & Cooke, M. S. (2019). Mycoplasma infection of cultured cells induces oxidative stress and attenuates cellular base excision repair activity. *Mutation Research/Genetic Toxicology and Environmental Mutagenesis,* 845, 403054.

Ji, Y., Karbaschi, M., & Cooke, M.S. Mycoplasma Infection Induces Oxidative Stress and Affects Cellular Base Excision Repair. In: 2018 *Annual Meeting Abstract Supplement, Society of Toxicology,* 2018. Abstract no. 1534a.

Perez, J., Ji, Y., Abdulwahed, A., Karbaschi, M., & Cooke, M.S. Development of a Simplified Cell Treatment Method Prior to Genotoxicity Assessment by the Comet Assay. In: 2018 *Annual Meeting Abstract Supplement, Society of Toxicology,* 2018. Abstract no. 2456a.

Alohaly, A. A., Ji, Y**.,** Cooke, M. S., & Karbaschi, M. (2017). Has the duration and temperature of lysis buffer been minimized for the comet assay? *The FASEB Journal*, *31*(1_supplement), lb54-lb54.